Evaluation of GCaMP3 Protoplasts for the Analysis of Ca^{2+} Signaling in Plant Immunity

by

Van Hong Phan

A thesis submitted in conformity with the requirements
for the degree of Master of Science

Department of Cell & Systems Biology
University of Toronto

Evaluation of GCaMP3 Protoplasts for the Analysis of Ca^{2+} Signaling in Plant Immunity

Van Hong Phan

Master of Science

Department of Cell & Systems Biology
University of Toronto

2018

Abstract

Ca^{2+} serves as a common second messenger in diverse eukaryotic cells. However, measuring *in planta* Ca^{2+} levels has been difficult. Recently, the fluorescence-based Ca^{2+} visualization indicator, GCaMP3 has emerged as a tool to visualize Ca^{2+} signals in plant cells; in particular, stress-related Ca^{2+} signals were successfully captured in GCaMP3 expressing leaf discs. In this study, the usage of GCaMP3 in protoplasts was evaluated. Upon stress-related stimuli, stress-induced Ca^{2+} signals were captured in *Arabidopsis thaliana* protoplasts using a fluorescence microscope and a plate reader. The signal pattern was faster and quicker but fundamentally similar to that of leaf discs, indicating that protoplasts can be used for Ca^{2+} visualization study. Furthermore, transfection of GCaMP3 in protoplasts was evaluated. Upon the bacterial elicitor flg22 treatment, Ca^{2+} signal was seen once by transfecting GCaMP3. Taken together, protoplasts can be used for investigating stress-induced Ca^{2+} signals using GCaMP3; however, transfection protocol has to be optimized.

Acknowledgements

First and foremost, I would like to thank my supervisor Keiko Yoshioka, for her amazing guidance and support as my supervisor. I am grateful to have been her student for the past two years. I would like to thank my committee members Daphne Goring and Alan Moses, for providing me with great feedback and guidance during our meetings. I would like to thank Wolfgang Moeder for keeping the lab running so smoothly.

I would like to acknowledge the many students to whom I have had the opportunity to work with in the Yoshioka lab. To Dr. Thomas DeFalco, whom laid down the initial groundwork for my project. Christine Cao, for being a great guide for not just biology but also yoga. Purva Karia, my office buddy that I can always count on for a laugh and great advice. Sonhita Chakraborty, whom helped me grow from her undergrad to a Master student. Angelica Miraples, the newest member to always cheer on the lab. Thanks to everyone in the Yoshioka/Nambara/Provart/Christendat/Goring lab for providing great advice. Special thanks to the Desveaux lab, Timothy Lo, Derek Seto, Madiha Khan, Bradley Leflamme, and Armand Miriam for the laughs and all the biological question pep talks. Thanks to Matthew Cumming and Anna van Weringh for the best hallway chats and biotech guidance.

Finally, I would like to thank my support group outside the lab, my family and friends. I would never be here without my parents, Hoa & Phuc, and my brother David, whom have helped me become the person I am today with their undying love and support. Arianne and Flora, the best ladies to follow and support in my plant story. Lastly I would like to thank Pierre, my biggest fan throughout this journey. I can’t wait for our next adventure together.

Table of Contents

List of Tables

List of Figures

Chapter 1

1 Introduction

1.1 Ca^{2+} signaling in plants

Ca^{2+} is a well-known universal second messenger in various eukaryotic signaling pathways. Many fundamental biological phenomena such as muscle contraction, neuronal transmission, and hormonal secretion are controlled by Ca^{2+} in animals (Carafoli., 2003). Eukaryotic cells actively maintain a low resting cytosolic Ca^{2+} concentration (~50-100nM) and sequester the majority of the Ca^{2+} from outside of the cell or subcellular compartments (mainly the ER and the vacuole). Ca^{2+} signals are generated by a combination of various channels, transporters, and pumps using extracellular and intracellular Ca^{2+} stores. In order to generate specific signals for each stimulus, specific spatial and temporal increases in cytosolic Ca^{2+} ($[Ca^{2+}]_{cyt}$) can be observed; these patterns are often called "Ca^{2+} signatures". Eukaryotic Ca^{2+} signaling involves three types of components. First, a signal must be recognized by a receptor at the plasma membrane or intracellularly. This signal recognition is associated with an increase in $[Ca^{2+}]_{cyt}$ through the activation or gating of one or more Ca^{2+} permeable cation channels. Next, this Ca^{2+} signal is interpreted by Ca^{2+}-binding sensor proteins, such as calmodulin (CaM), CaM-like proteins (CML), Ca^{2+}-dependent protein kinases (CDPKs), and calcineurin B-like proteins (CBLs) (DeFalco *et al.*, 2010; Batistič and Kudla., 2012). Lastly, these Ca^{2+} sensors transduce the signal into the relevant cellular response such as modulating gene expression. In plants, Ca^{2+} signaling is involved in many diverse processes where it mediates environmental stimuli and developmental processes or cues. One important process is plant immunity (Sanders *et al.*, 2002; Kudla *et al.*, 2010; Seybold *et al.*, 2014).

1.2 Ca^{2+} in plant immunity

Transient changes in $[Ca^{2+}]_{cyt}$ are rapidly generated upon diverse stimuli, where they mediate responses to developmental cues (eg. reproduction, circadian clock), abiotic stimuli (eg. cold shock, drought, wounding) and biotic stimuli (eg. infection with pathogenic, symbiotic microorganisms and insects). Plants differ from animals, where they lack an adaptive immune system, therefore, they must respond to biotic stresses at the cellular level mediated by receptor

proteins (Jones and Dangl., 2006). Plant immunity can be classified into two categories: pattern-triggered or PAMP-triggered immunity (PTI), and effector-triggered immunity (ETI). Plasma membrane localized pattern recognition receptors (PRRs) recognize conserved molecular patterns called microbe (pathogen)-associated molecular patterns (MAMPs/PAMPs) and endogenously-derived damage-associated molecular patterns (DAMPs). Activation of these receptors leads to PTI (Zipfel, 2008; Jones and Dangl., 2006). ETI, on the other hand, is activated by resistance (R) proteins, which are largely represented by nucleotide-binding leucine-rich repeat (NB-LRR) proteins that recognize effector proteins secreted by pathogens. ETI often induces a type of programmed cell death (PCD), denoted as the hypersensitive response (HR) (Jones and Dangl., 2006).

Both PTI and ETI involve many overlapping signaling components, such as salicylic acid (SA) and MAP-kinase (MAPK) cascades (Coll *et al.*, 2011). In addition, previous studies have shown changes in ion fluxes as a well-known early response to pathogen recognition in plants, likely for both ETI and PTI. These ion flux changes involve anion efflux and cation $[Ca^{2+}]_{cyt}$ influx (Seybold *et al.*, 2014) (Figure 1). Extensive efforts showed that upon treatment of P/MAMPs an elevation of $[Ca^{2+}]_{cyt}$ level occurred (Chandra and Low., 1997; Lecourieux., 2002; Ranf *et al.*, 2008; Maintz *et al.*, 2014). Furthermore, it has been known that Ca^{2+} plays an essential role in immunity, since relevant gene mutation or pharmacological inhibition of Ca^{2+} signals can obstruct downstream events such as reactive oxygen species (ROS) production upon pathogen infection or pathogen related treatment (Chandra and Low., 1997; Seybold e*t al.*, 2014). ROS production after pathogen infection is called an oxidative burst and is essential for immunity activation (Chandra and Low., 1997; Maintz *et al.*, 2014). Pre-treatment with the Ca^{2+} channel inhibitor, ruthenium red, reduces Ca^{2+} signals generated by oligogalacturonic acid (OGA) in tobacco cells (Chandra and Low., 1997). OGA is a well-known elicitor of an oxidative burst through the activation of phospholipase C, which causes downstream signaling events to release internal Ca^{2+} stores, showing a relationship between Ca^{2+} levels, and ROS production.

Although Ca^{2+} signaling has been reported to play an important role in immunity and in other stress-response signaling pathways, studies of *in planta* Ca^{2+} signaling have been

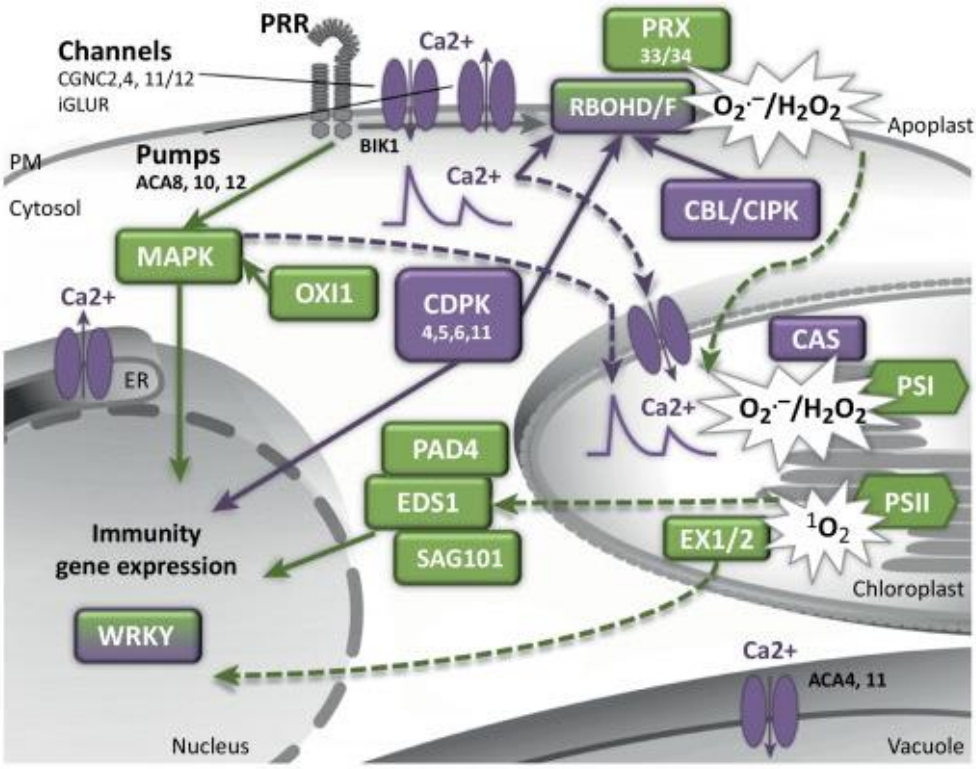

Figure 1: Ca^{2+} signaling pathway during plant immunity.

Calcium signaling pathways during plant immunity. A fast response is triggered upon PAMP perception by PRRs signaling the concerted action of calcium (Ca^{2+}) channels and transporters that generate a $[Ca^{2+}]_{cyt}$ flux. Calcium-dependent protein kinases (CDPKs), upon activation by the Ca^{2+} flux, together with a mitogen-activated protein kinase (MAPK) cascade will trigger immunity gene expression in the nucleus, in which, for example, WRKY transcription factors play important roles. MAP kinases are regulated by the ROS sensory kinase oxidative signal-inducible 1 (OXI1). At the same time, Ca^{2+} flux and phosphorylation by Botrytis-induced kinase 1 (BIK1), CDPKs, and calcineurin B-like protein (CBL)/CBL-interacting protein kinase (CIPK) modules can enhance the activity of plasma membrane localized respiratory burst oxidase homologs (RBOHs) D and/or F (RBOHD/F) to produce apoplastic ROS (O2•−/H2O2). Peroxidases 33 and 34 (PRX33/34) contribute to apoplastic ROS generation for the oxidative burst. Within 20 min of pathogen perception, a Ca^{2+} flux is generated in the chloroplast, which is regulated by the thylakoid associated calcium-sensing protein (CAS). Pathogen perception might be signaled to the chloroplast by a MAPK cascade, direct transfer of calcium from the cytosol to the chloroplast or H2O2 coming from the oxidative burst (or a combination thereof). Downstream retrograde signaling to the nucleus might involve the ROS 1O2 (mainly generated by photosystem II [PSII]) and O2•− (mainly generated by photosystem I [PSI]). Executer1 and 2 (EX1/2) act downstream of 1O2 to alter nuclear gene expression. The central immune regulator enhanced disease susceptibility 1 (EDS1) has been implicated downstream of chloroplastic O2•− and interacts with phytoalexin deficient 4 (PAD4) and Senescence-Associated gene 101 (SAG101) as heterodimers to alter nuclear immunity gene expression (adapted from Stael *et al.*, 2015).

technically difficult due to two issues: 1. masking of small $[Ca^{2+}]_{cyt}$ changes due to high levels of apoplastic Ca^{2+} and 2. signal transduction triggering intracellular Ca^{2+} release from organelles, which some Ca^{2+} methodologies cannot analyze due to no net change in cellular Ca^{2+} levels (Chandra and Low., 1997).

1.3 Cyclic Nucleotide-Gated Ion Channels (CNGCs)

Although the importance of Ca^{2+} signals in plants has been known for a long time, the identity of the Ca^{2+} channels in plants has been obscure (Berridge *et al*., 2000; Edel *et al*., 2017; Moeder *et al*., 2018). Although plants do not have the counterpart of some animal Ca^{2+}channels, such as voltage-dependent Ca^{2+} channels (VDCCs) and transient receptor potential (TRP) channels, they do have other Ca^{2+}-permeable channel candidates. One family of ligand-gated Ca^{2+} permeable channels in plants is the Cyclic Nucleotide-Gated Ion Channel (CNGC) family. CNGCs are non-selective cation channels with the following core structural characteristics: a cytosolic N- and C-terminus, six transmembrane helices (S1-S6), a pore-forming region between S5-S6, a linker region following S6, and a C-terminal cyclic nucleotide-binding domain (CNBD) (Kaupp and Seifert., 2002; Matulef and Zagotta., 2003). CNGCs were first identified in mammalian vertebrate photoreceptors and olfactory sensory neurons (Zagotta *et al.*, 1996). The mammalian CNGCs are regulated by the direct binding of cyclic nucleotide monophosphates (cNMPs), such as cyclic adenosine-3', 5' monophosphate (cAMP) and/or cyclic guanosine-3',5' monophosphate (cGMP) (Kaupp and Seifert., 2002). However, the regulation of plant CNGCs by cNMPs is still controversial (Moeder *et al.*, 2018).

1.4 CNGCs in plants

The first plant CNGCs were discovered in barley, as a CaM-binding protein (Schuurink *et al*., 1998). The model plant species *Arabidopsis thaliana* harbours 20 members of the CNGC family (Mäser *et al*., 2001). They are divided into 4 groups based on their sequence similarity (Group I, II, III, and IVa/IVb). Three CNGC mutants were isolated based on their immunity-related phenotypes: the *defense, no death,* (*dnd1*) (Clough *et al*., 2000), *dnd2/HR-like lesion mimic 1 (hlm1)* (Jurkowski *et al*., 2004), and *constitutive expressor of pathogenesis-related genes 22* (*cpr22)* (Yoshioka *et al*., 2001, 2006). The causal mutation of *cpr22* is a gain-of-function mutation in *CNGC11* and *CNGC12*, whereas that of *dnd1* and *dnd2* mutants are caused

by loss-of-function mutations in their corresponding *CNGCs* alleles (*CNGC2* and *CNGC4* for *dnd1* and *dnd2*, respectively) (Clough *et al*., 2000; Balague *et al*., 2003; Jurkowski *et al*., 2004; Yoshioka *et al*., 2006). *CNGC2* and *CNGC4* both belong to group IVb, and their association as a heterotetramer *in planta* has been reported (Chin *et al*., 2013). *dnd1* was isolated through a mutant screen for its inability to trigger HR cell death with an avirulent pathogen infection (Yu *et al*., 1998; Clough *et al*., 2000). Interestingly, PAMP-induced Ca^{2+} influx activated by the PAMP, lipopolysaccharide (LPS) and by the DAMP, plant elicitor peptide 3 (PEP3) is also suppressed in *dnd1* (Ali *et al*., 2007; Ma *et al*. 2012). *cpr22* has a 3 kb deletion in of *CNGC11* and *CNGC12*, causing a chimeric fusion of *CNGC11* and *12*, referred as *CNGC11/12* (Yoshioka *et al*., 2006). The expression of chimeric *CNGC11/12* has been shown to induce constitutive defense responses, such as spontaneous HR-like PCD and elevated levels of salicylic acid. (Yoshioka *et al*., 2006; Urquhart *et al*., 2007) (Figure 2). The suppression of *CNGC11/12*-induced PCD by Ca^{2+} inhibitors but not K^+ inhibitors supports the importance of Ca^{2+} in *cpr22*-induced HR-like PCD (Yoshioka *et al*., 2006; Urquhart *et al*., 2007), although the wild-type *CNGC11* and *CNGC12* channels as well as CNGC11/12 conduct both Ca^{2+} and K^+ in yeast complementation assay. Together, the aforementioned data suggests that *CNGC11/12* induces autoimmunity phenotype via its Ca^{2+} conducting activity and it can be used as a tool to understand CNGC-mediated Ca^{2+} signaling.

1.5 Ca^{2+} visualization

For a long time there has been an interest to develop methods to monitor Ca^{2+} fluxes at a high temporal resolution, however, this has been shown to be difficult in plants. In animal cells Ca^{2+}-sensitive fluorescent dyes such as Fura-2 and Indo-1 are often used to monitor Ca^{2+} signal activation. However, they are not suitable for plants due to their difficulty to permeate the cell wall well. In addition, their potentially toxic effects in plant cells are a concern to study stress responses. This, alternative approaches have been sought to monitor Ca^{2+} in plant cells. Studies using genetically encoded Ca^{2+} indicators (GECIs) to visualize cellular Ca^{2+} levels have overcome the aforementioned obstacles. For example, the aequorin-expressing transgenic plants partially resolved the limitation of the need to deliver the dye into the cytosol (Knight *et al*., 1993). However, the aequorin luminescence system requires the exogenous application of its cofactor, coelenterazine, and in addition, it requires a specific luminometer for detection (Knight

and Knight., 1995; Maintz *et al*., 2014). On the contrary, fluorescence-based GECIs do not require a substrate (Whitaker., 2012). Usually, these sensors utilize a chimeric fusion of one or more fluorescent proteins to the Ca^{2+} -binding protein calmodulin (CaM) and a Ca^{2+} dependent CaM-binding domain M13 peptide (Figure 3). In the case of ratiometric sensors such as the Yellow Cameleon (YC), a Ca^{2+}-dependent Förster resonance energy transfer (FRET) effect allows us to monitor *in vivo* Ca^{2+} concentration changes by the ratio between two emission wavelengths, however this requires use of a confocal microscope for detection (Horikawa *et al*., 2010; Monshausen, 2012). GCaMPs, on the other hand, are intensity based sensors, which upon Ca^{2+} binding at physiological concentrations, display an increase in fluorescence intensity (Nakai *et al*., 2001) (Figure 3). Thus, visual examination of transgenically expressed GCaMP in plants can be performed using a regular fluorescence microscope with a narrow emission filter for eGFP.

In the Yoshioka lab, a previous Ph.D. student Dr. Thomas DeFalco had generated GCaMP3 and YC nano65 expressing *Nicotiana* species and analyzed Ca^{2+} signal activation using several PAMPs and a number of inhibitors (DeFalco *et al*., 2017). Through this analysis, he has used a plate reader system to quantify Ca^{2+} signals. The combination of visual recording and quantification is a powerful tool to analyze Ca^{2+} signaling in plants.

1.6 Thesis Objectives

My objective in this Master's thesis was to evaluate usage of GCaMP3 in protoplasts and develop the protocol to analyze stress related Ca^{2+} signaling, with an emphasis on pathogen defense and analyze the involvement of possible defense-related components in Ca^{2+} signals. My thesis project contains two aims:

My first aim was to test if GCaMPs can be used in protoplasts to monitor Ca^{2+} signals upon biotic and abiotic stresses. Here, I explore the use of *A. thaliana* leaf mesophyll protoplasts, derived from a stable transgenic line expressing a GCaMP3. Since the cell wall is removed, which definitely causes stress, it has been questioned if protoplasts are suitable to capture stress signal activation properly (Yamazaki *et al*., 2009; Maintz *et al*., 2014). However, PAMP-induced Ca^{2+} signals have been reported using protoplasts by the aforementioned aequorin and it was

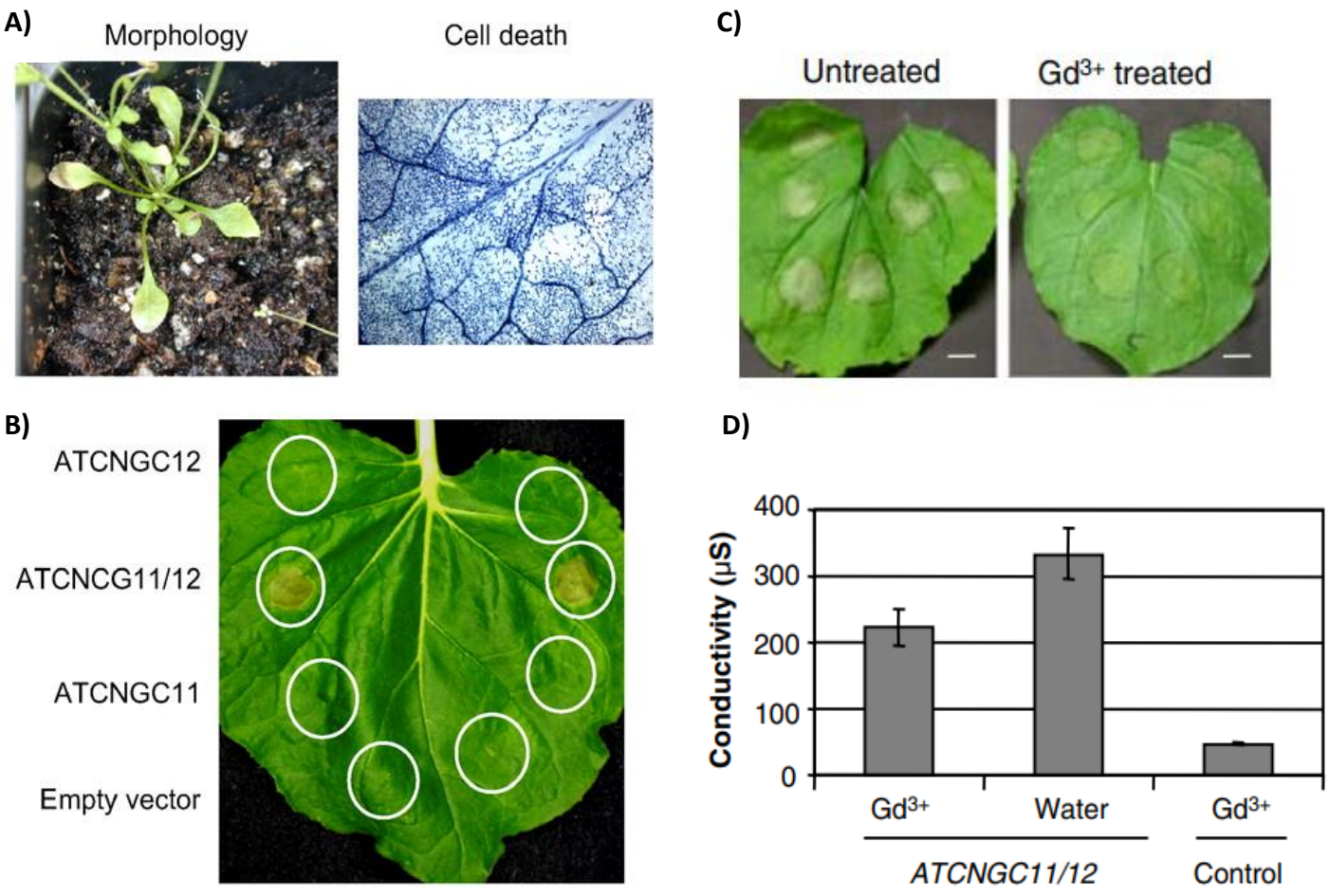

Figure 2: *AtCNGC11/12*-induced cell death expressed in *N. benthamiana* is inhibited by Ca^{2+} channel blockers.

(A) Expression of *AtCNGC11/12* induces *cpr22* phenotypes (stunted growth and spontaneous cell death) and (B) transient expression of *AtCNGC11/12* but not *AtCNGC11*, or *12* induces HR-like cell death (adapted from Yoshioka *et al.*, 2006).
(C) Ca^{2+} channel inhibitor gadolinium chloride (Gd^{3+}) inhibits *AtCNGC11/12*-induced cell death (adapted from Urquhart *et al.*, 2007).

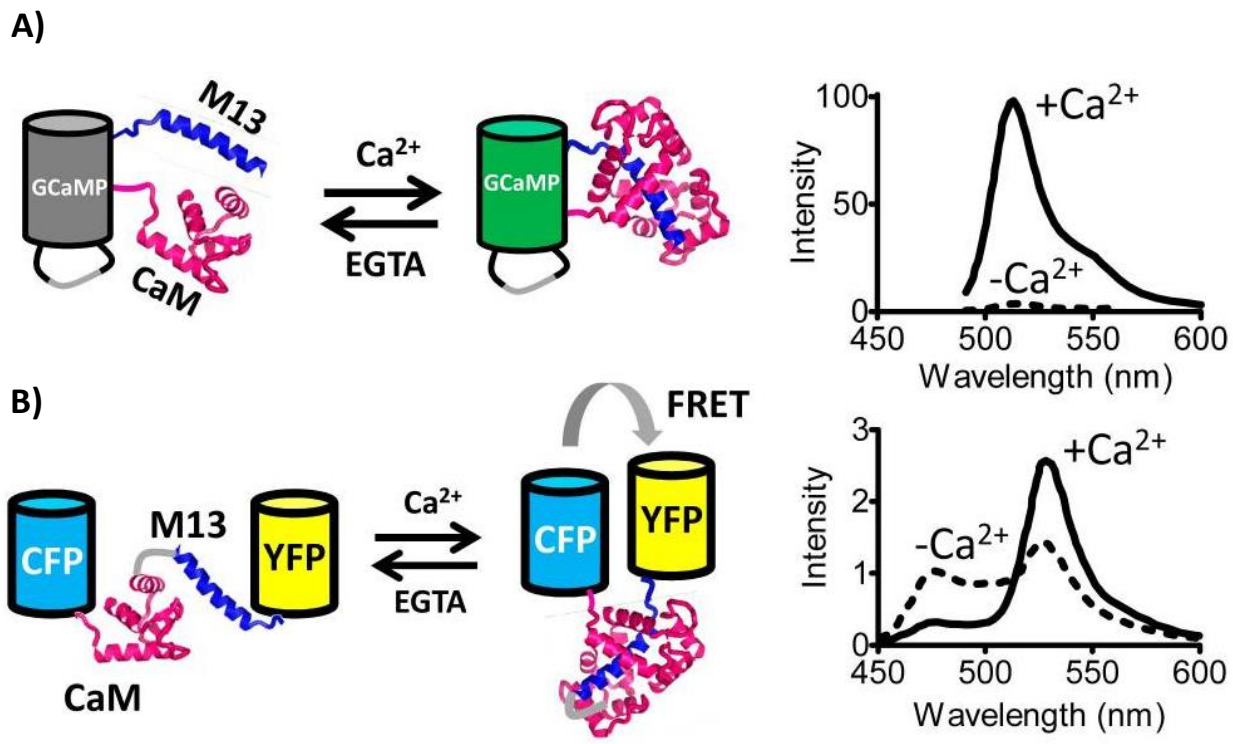

Figure 3: Intensity-based and FRET-based genetically encoded Ca^{2+} indicators.

(A) GCaMP sensor is intensity based, where upon Ca^{2+} binding, the increase in fluorescence intensity can be measured. (B) Cameleon sensor is utilized in Förster resonance energy transfer (FRET) allows for in vivo Ca^{2+} concentration to be calculated from the ratio between two emission wavelengths. Ca^{2+} binds to M13, which enables calmodulin to wrap around the M13 domain. This brings the two GFP-variant proteins closer to each other, which increases FRET efficiency between them (adapted from Lindenburg and Merkx., 2014).

shown that there is no significant difference between protoplasts and whole plant responses (Maintz *et al*., 2014). Thus, in this project, I aim to determine whether GCaMPs in protoplasts can capture stress-induced Ca^{2+} signal.

As discussed, GCaMPs have a significant advantage over Ca^{2+}-sensitive dyes to visualize the Ca^{2+} signals in plants and can be used to identify possible signaling components with their mutants. However, to test alterations in Ca^{2+} signaling in mutant backgrounds, we have to introduce GCaMPs genetically into each mutant background by cross-pollination or transformation, which takes a significant amount of time and effort. Transfection of GCaMPs into protoplasts can theoretically help us save time and effort. In addition, genes of interest can be silenced by RNAi or CRISPR/Cas9 by transfection of protoplasts isolated from GCaMP wild-type plants. Thus, establishing the transfection of protoplasts will provide us a powerful tool.

My second aim is to further analyze Ca^{2+} signaling components involved in pathogen recognition. DeFalco *et al* (2017) have tested two types of PAMPs, flg22, and elf18, which are epitope peptides derived from flagellin and Elongation Factor Tu (EF-Tu) of bacterial pathogens, that are recognized by the PRRs, FLS2, and EFR, respectively (Bektas and Eulgem., 2015; Zipfel., 2008). Chitin is another well-studied PAMP from fungal pathogens and CERK1 and LYM2 have been identified as its receptor (Yamada *et al*., 2016). All of these PAMPs induce PTI. On the other hand, ETI is induced by effector proteins and usually associated with HR cell death. HR cell death is also induced by certain pathogen toxins, such as Fumonisin BI (FBI) (Wang *et al*.,1996; Asai *et al*., 2001) and also the chimeric CNGC, CPR22 (CNGC11/12, Yoshioka *et al*., 2006).

The previous Ph.D. student Dr. Huda Abdel-Hamid conducted a chemical screening for suppression of CNGC11/12-induced HR-like cell death and identified several chemicals from the LATCA (Library of AcTive Compounds on Arabidopsis) chemical library (http://cutlerlab.blogspot.com/2008/05/latca.html) that can suppress CNGC11/12-induced lethality in *cpr22* mutants (Abdel-Hamid *et al*., 2011) (Figure 4). Some of them are Ca^{2+} channel blockers indicating that CNGC11/12 activates Ca^{2+} signal to induce autoimmunity. In addition, it has been reported that CNGC11/12-induced cell death is Ca^{2+}-dependent (Urquhart *et al*., 2011),

thus the chemicals identified in the screen can be great tools to observe Ca^{2+} signals induced by pathogen resistance inducers. Therefore, I aim to analyze the combination of these chemicals and various inducers such as flg22, chitin, and FB1. In addition, a *cpr22* expressing GCaMP3 line has been generated, thus I analyzed *cpr22*-mediated Ca^{2+} signaling using GCaMP3 and the chemicals that were identified by Abdel-Hamid *et al.* (2011). These analyses ultimately can reveal similarities and difference between PTI and ETI related Ca^{2+} signals. Currently, there is no knowledge about the difference of Ca^{2+} signals between these two immune responses.

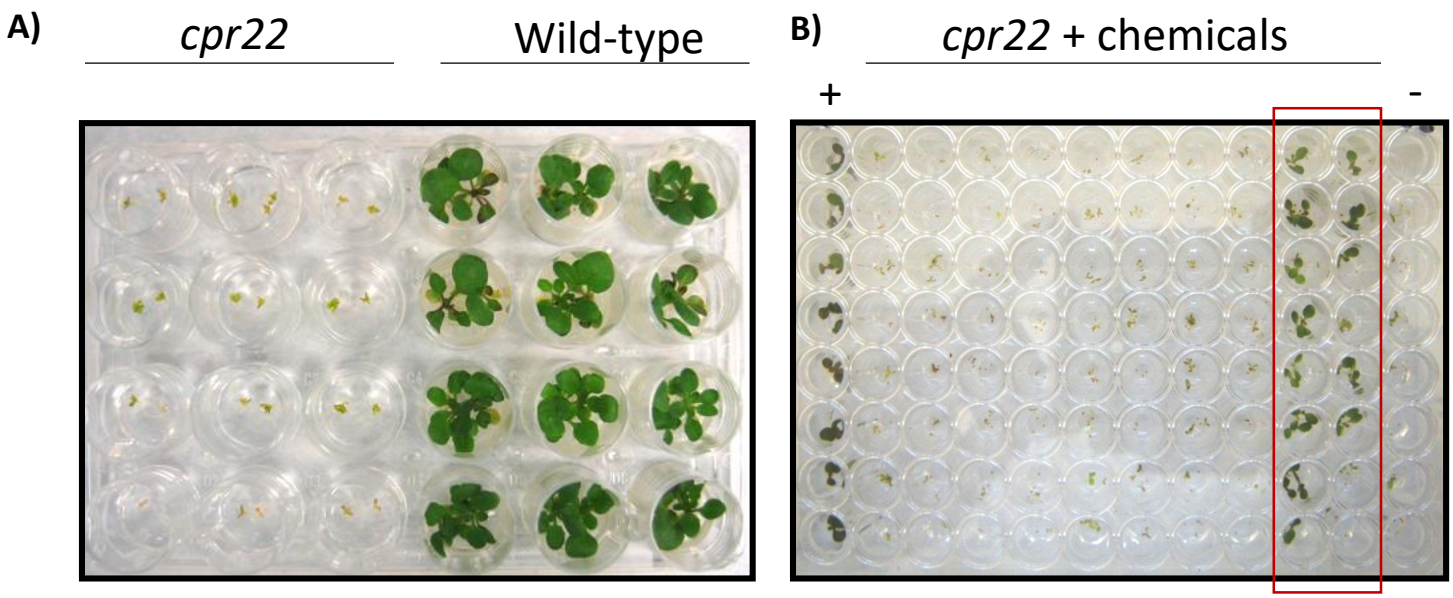

Figure 4: Chemical library screen identified 13 chemicals that suppress *AtCNGC11/12*-induced HR-like cell death.

(A) *cpr22*-mediated lethality (left) and wild-type (right) *A. thaliana* seedlings grown on Murashige Skoog agar medium. (B). High throughput screening of the LATCA chemical library in 96-well plates. Red box indicates surviving plants. (+) indicates wild-type plants without chemicals. (-) indicates *cpt22* homozygous plants without chemicals (adapted from Abdel-Hamid *et al.*, 2011).

Chapter 2

2 Materials and Methods

2.1 Plant Materials and Growth Conditions

Arabidopsis thaliana and *Nicotiana benthamiana* used for experiments were grown for approximately 4-5 weeks on Sunshine mix #1 soil (Sun Gro Horticulture Canada) in a growth chamber under 9/15h light/dark regimen at 22°C (day) and 20°C (night). For seed production, 5-week old plants were moved to a growth chamber and grown under 16/8 h light/dark growth conditions at 22°C (day) and 20°C (night). *cpr22* GCaMP3 *A. thaliana* plants were grown in a growth chamber at 26°C (day/night).

2.2 Protoplast isolation

Arabidopsis protoplast isolation: Protoplast isolation was modified from the Yoo *et al*. 2007. Leaves were cut into 0.5-1mm leaf strips with fresh razor blades without wounding. 10-20 leaves were digested in 5-10 ml an enzyme solution (1.5 % cellulose, 0.4% macerozyme, 0.4M Mannitol (1M stock), 20 mM KCl (1M stock), 20 mM MES, pH 5.7 (0.5M stock), 10 mM $CaCl_2$ (1M stock). The leaf strips were submerged in the enzyme solution in a petri dish and digested overnight for 16-18 hours. The protoplasts were released by gentle shaking of the petri dish for 1-5 min. The enzyme containing the protoplasts were filtered through a 100 μm nylon mesh. The solution was spin at 1000 rpm for 2 min to pellet the protoplasts in a round bottom 50 ml Falcon tube. The supernatant was removed and the protoplasts were re-suspended in washing/incubation (WI) buffer (0.5M Mannitol, 4mM MES, pH 5.7, and 20nM KCl) for microscopy and quantification assays or W5 solution (154 mM NaCl, 125 mM $CaCl_2$, 5 mM KCl, 2 mM MES pH 5.7) for PEG transfection at 2 x 10^5 protoplasts/ml.

Nicotiana protoplast isolation: Protoplast isolation of *Nicotiana benthamiana* was modified from Current Protocols in Microbiology 16D.2.2, Supplement 4. Protoplasts were isolated similarly to *Arabidopsis, Nicotiana* protoplasts were incubated in K3 media (0.4M Sucrose in MS, 1.5% cellulose/0.4% macerozyme). *Nicotiana* protoplasts were washed twice

with Nicotiana wash buffer (2.75% $CaCl_2$, 0.5% MES, pH. 5.6) before re-suspension in WI buffer for microscopy and quantification assays.

2.3 Plasmid Construction

The vector pUC18: GCaMP3 plasmids used for the transfection was constructed in several stages. The GCaMP3 insert was digested from the pBIN20:GCaMP3 plasmid using *BamH1* and *StuI* restrictive enzyme sites. The CNGC20 construct was similarly removed from pUC18:CNGC20 using *BamHI* and *StuI* restriction enzyme sites. GCaMP3 construct was cloned into the pUC18 construct using T4 ligase (Thermofisher). The pUC18:GCaMP3 constructs were positively identified by polymerase chain reaction and gel electrophoresis, and then sequenced using the primers listed in Table 1 to the TCAG sequencing facility.

TABLE 1: LIST OF PRIMERS

PCR REACTION	TOY-BAMH1-F – 5’ – ATG GAT CCA TGG GTT CTC ATC ATC – 3’.
	TOY-STUI-R – 5’ – CAA GGC CTT CAC TTC GCT GTC ATC ATTT– 3’.
SEQUENCING	EGFP-F – 5’ – GAC GTA AAC GGC CAC AAG TT – 3’
	EGFP-R – 5’- GAA CTC CAG CAG GAC CAT GT – 3’

2.4 Transfection of GCaMP3 into protoplasts

Steps of transfection were carried out at 23°C and optimized for GCaMP3 plasmid transfection. Plasmid DNA was extracted following the alkaline maxi prep protocol provided by the Goring lab. 10 µl of DNA (1-2 mg of plasmid DNA) was added to a 1.5 ml Eppendorf tube. 100 µl protoplasts are added to the microfuge tube and mixed. 110 µl of PEG/Ca^{2+} solution (4 g PEG4000 by Fluka, 3 ml H_2O, 2.5 ml 0.8M Mannitol, 1 ml 1M $CaCl_2$) was added to the tube and mixed well. Samples were incubated at 23°C for 30 min. The sample was diluted with 0.44 ml of W5 solution and mixed well. Samples were spin at 1000 rpm for 1 min. PEG transfection

solution was removed and the pellet was re-suspended gently with 100 µl W5 buffer. Protoplast solution was added to 1 ml of W5 (final volume of 1.1 ml) in a 6 well plate and incubated for 6-16 hours.

2.5 Preparation of chemical stocks

flg22 and elf18 peptides were synthesized commercially and dissolved in ddH_2O, then diluted to 1000 x stock (100 µM). ATP, $GdCl_3$, neomycin, and diethylstilbestrol were all dissolved in ddH_2O as 1000x stocks (100 mM for ATP, $GdCl_3$, and 50 mM for Neomycin) and 100x stock for diethylstilbestrol (10 mM). DPI and nifedipine were dissolved in dimethyl sulfoxide (DMSO) to stock concentrations of 10mM. Chitin (Calbiochem) stocks were prepared fresh, by first grinding powder with mortar and pestle on ice for 5 min, after which a half-final volume of autoclaved ddH_2O was added and the mixture was ground for an addition 5 min. The resulting slurry was diluted to a final stock concentration of 10 mg ml^{-1} and sonicated for 10 minutes before use. L-glutamate was prepared fresh for use in ddH_2O (100 mM).

2.6 Quantification of Ca^{2+} signals and inhibitor assays

Protoplasts were isolated from GCaMP3-expressing transgenic plants and adjusted to 2.5 x 10^5 cells/ml. 50 µl of the protoplast solution was equilibrated in 50 µl of either WI buffer, or WI + inhibitor (100 µM $GdCl_3$, neomycin, nifedipine, or DPI). For the leaf disc assay, 10 x 0.5cm leaf discs from 5-week old plants were equilibrated abaxial side up in 100 µl of ddH_2O, or ddH_2O + inhibitors (100 µM $GdCl_3$, neomycin, nifedipine, or DPI) for 2-4 hours in a Greiner 96-well flat black plate. Following equilibration, 100µl of ddH_2O (leaf disk control), WI buffer (protoplast control) or 100 nM of flg22 in ddH_2O (for leaf discs) or WI buffer (for protoplasts) was added, Ca^{2+} signal was immediately measured using the TECAN Infinite M1000 Pro plate-reader. Absolute fluorescence values for each experiment were normalized to the untreated control value F/F_{eq} (where F was measured fluorescence and F_{eq} was averaged measurement for control at the final resting time point).

2.7 Real-time Ca^{2+} imaging via fluorescence microscopy

Flg22-induced Ca^{2+} measurements were recorded on a Leica M216F stereo fluorescence microscope using a Leica DFC 7000T CCD camera controlled by LasX software. The GCaMP3

signal was visualized using the ET-GFP emission/excitation filter (Leica Microsystems). Images were captured every 10 seconds during flg22-induction experiments.

Chapter 3

Some data were published in:

Ca^{2+} to the rescue – Ca^{2+} channels and signaling in plant immunity. Moeder W., Phan V., Yoshioka K. (2018). *Plant Sci*. doi: 10.1016/j.plantsci.2018.04.012

Author contributions: V.P. produced Figure A1.1.

And

Using GCaMP3 to study Ca2+ signaling In *Nicotiana* species. DeFalco TA., Toyota M., Phan V., Karia P., Moeder W., Gilroy S., Yoshioka K. (2017). *Plant Cell Physiol*. 0: 1-12

Author contributions: V.P. performed Figure 14.

3 Results

3.1 Isolation of protoplasts from transgenic *A. thaliana* and *N. benthamiana* carrying GCaMP3

Protoplasts were successfully isolated from wild-type and GCaMP3-expressing *Arabidopsis* and *Nicotiana benthamiana* plants (Figure 5). The pictures taken by a stereo-fluorescence microscope showed no fluorescence signal in wild-type protoplasts, whereas a clear signal in GCaMP3 protoplasts was observed (Figure 5). The Ca^{2+} signal detected is the basal level without any stimulation. To observe the signal in higher resolution, fluorescence signals were observed by a confocal microscope. As shown in Figure 6, a clear basal GFP signal was observed in GCaMP3 protoplasts but not wild-type protoplasts, indicating that the protoplast isolation procedure does not interfere with the signals and that the GFP signal is localized to the cytosol.

3.2 PAMP and DAMP-induced Ca^{2+} flux in *A. thaliana* GCaMP3 protoplasts

To analyze Ca^{2+} signals activated by various stimuli in protoplasts, quantitative analysis was conducted upon treatment of biotic stress-related PAMPs, such as flg22, elf18, and chitin. As mentioned previously in the introduction, the bacterial protein flagellin contains a well-studied conserved 22 amino acid epitope (flg22), which activates PTI, while elf18 peptide is the conserved epitope from bacterial EF-Tu (Zipfel., 2008). Chitin, a well characterized PAMP, is a

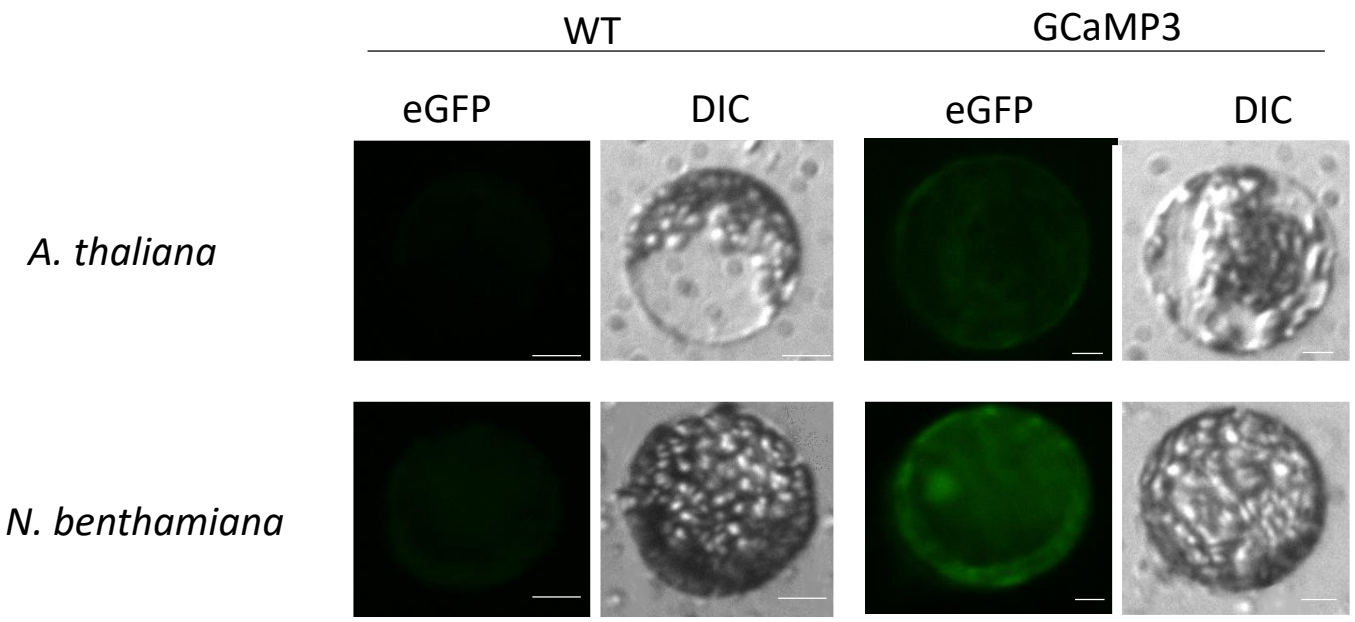

Figure 5: Basal fluorescence of Ca^{2+} indicator GCaMP3 in transgenic protoplasts compared to wild-type protoplasts using the fluorescence microscope.

Protoplasts from wild-type and transgenic plants carrying GCaMP3. Top: *Arabidopsis thaliana*. Bottom: *Nicotiana benthamiana.* Left: Wild-type protoplasts. Right: Transgenic GCaMP3 protoplasts. Scale bar = 10µm.

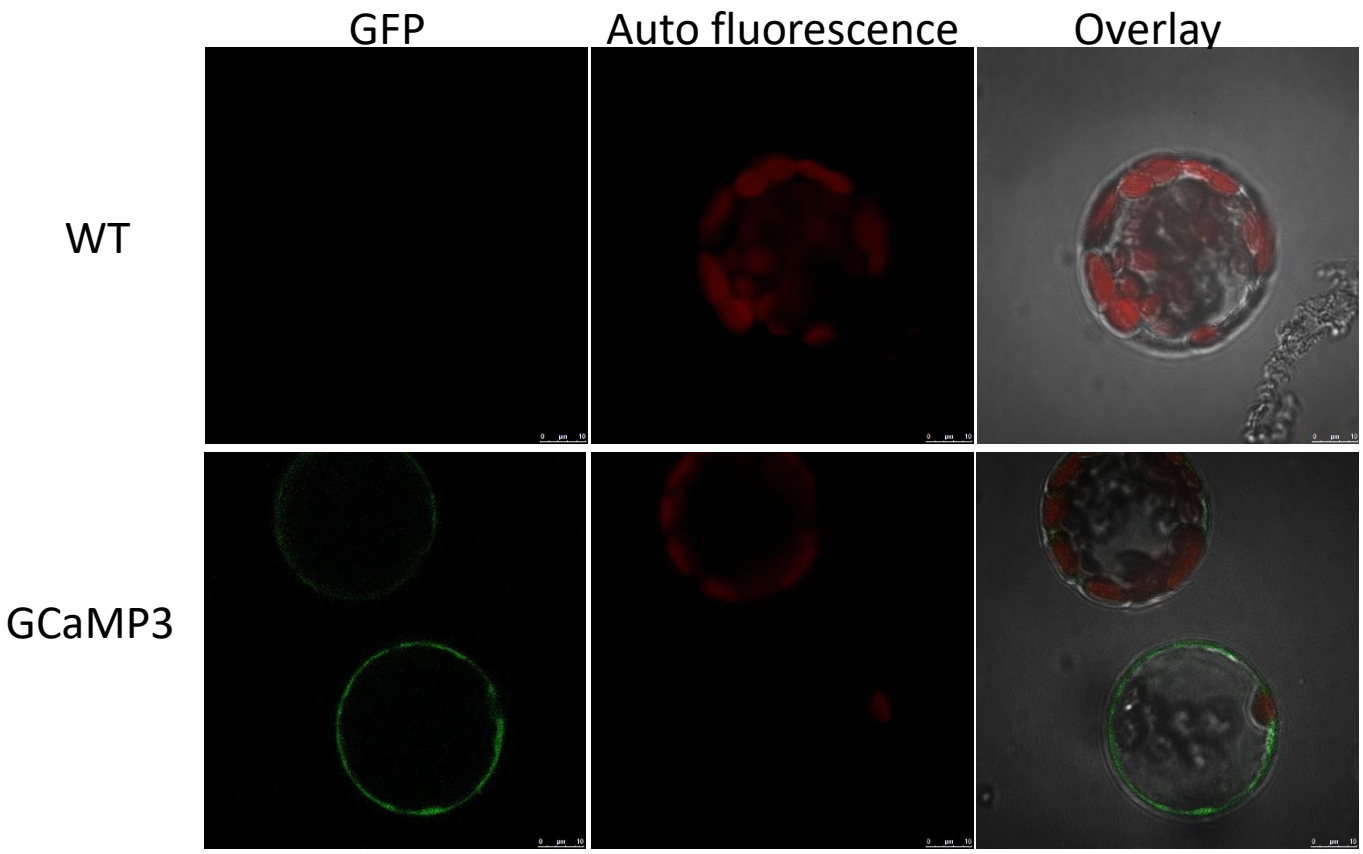

Figure 6: Basal fluorescence of GCaMP3 *A. thaliana* protoplasts using a confocal microscope.

Protoplasts from wild-type and transgenic plants carrying GCaMP3. Top: Wild-type *Arabidopsis thaliana* protoplasts. Bottom: Transgenic GCaMP3 *Arabidopsis thaliana* protoplasts. Scale Bar =10µm. 63X 3 zoom

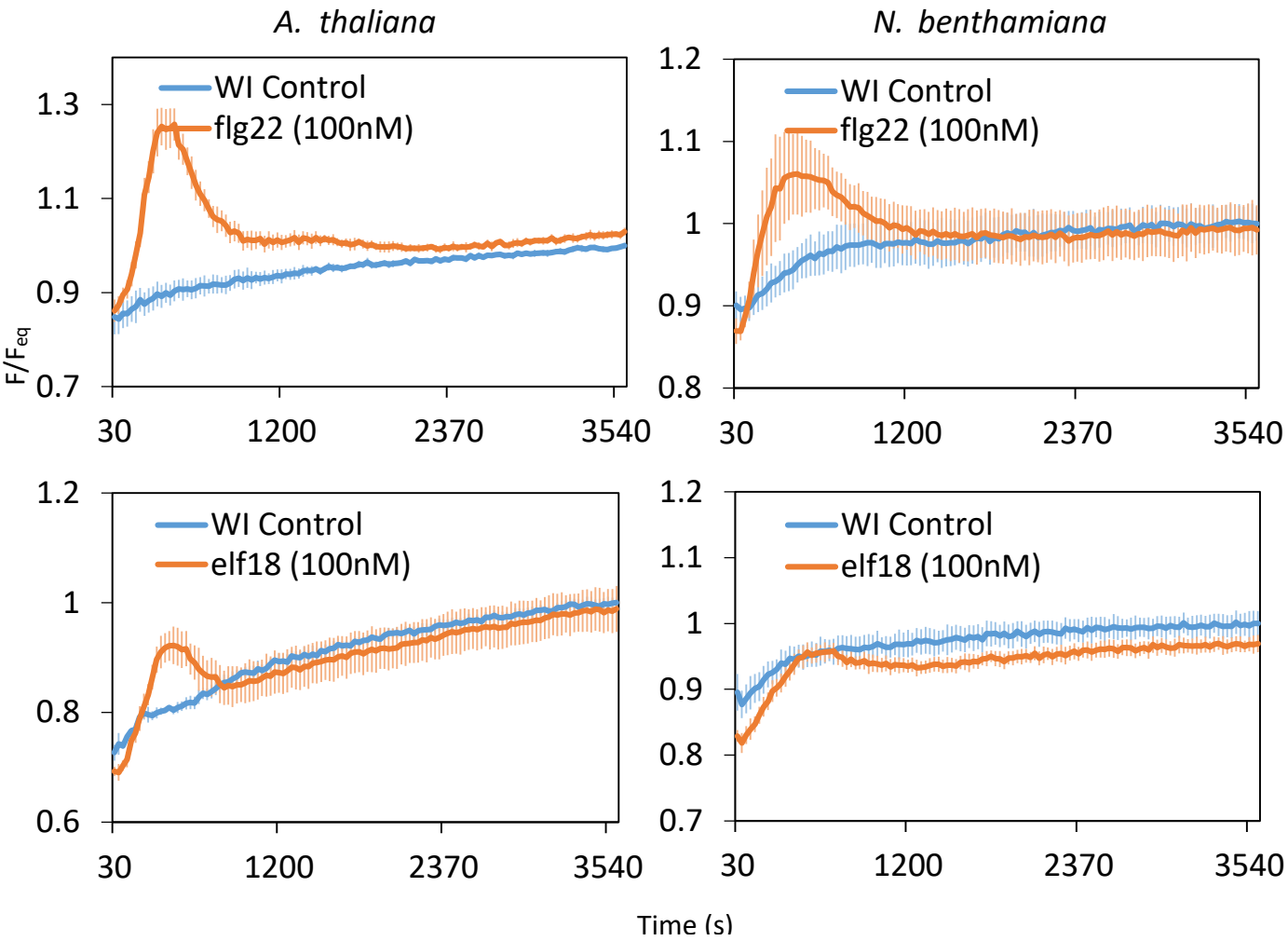

Figure 7: PAMP-triggered Ca^{2+} flux in *A. thaliana* and *N. benthamiana* GCaMP3 protoplasts.

Protoplasts were treated with 100nM flg22 (left panels) or 100nM elf18 (right panels). WI buffer was used as a negative control. Error bar represents ±SE. n=3. The experiment was conducted at least three times with similar results.

major component of the fungal cell wall, and a polymer of N-acetyl D-glucosamine (Zipfel., 2008). Additionally, other compounds such as plant-derived peptides and ATP can act as DAMPs in plants and can also induce Ca^{2+} signals (Ranf *et al*., 2011; Tanaka *et al*., 2014). Absolute fluorescence values for each experiment were normalized to the untreated control value F/F_{eq} (where F was measured fluorescence and F_{eq} was averaged measurement for control at the final resting time point). As expected, the plate-reader detected flg22 and elf18-induced Ca^{2+} fluxes in protoplasts, with a max peak at 4.5, and 7.5 F/F_{eq}, respectively (Figure 7). The chitin-induced Ca^{2+} signals were also higher than elf18, and the time to reach to the max peak was longer, at 9.5 min (Figure 8). The time to reach to the max peak of the ATP-induced Ca^{2+} signal was the quickest at 4 minutes (Figure 9). This demonstrates that *A. thaliana* protoplasts maintain functional receptors for these PAMPs and DAMPs that can induce downstream Ca^{2+} signals.

3.3 PAMP-triggered Ca^{2+} flux in *N. benthamiana* GCaMP3 protoplasts

Similarly to the *A. thaliana* protoplasts, the biotic stress-related stimuli were tested in *N. benthamiana* GCaMP3-expressing protoplasts. As expected, flg22 was able to induce a Ca^{2+} flux in our assay, aligning with the fact that *N. benthamiana* has a functional receptor FLS2 for flg22 (Figure 7). The timing of activation of the signal was similar to that in *A. thaliana* protoplasts. No Ca^{2+} signal was observed in non-transgenic control samples. Conversely, it was also expected that elf18 should not induce a Ca^{2+} signal in *N. benthamiana*, as *N. benthamiana* does not have the cognate EFR receptor (Zipfel, 2008). flg22-induced Ca^{2+} signals in both *A. thaliana* and *N. benthamiana, w*ith a max peak at 4 and 7 minutes, respectively, though I observed a stronger max peak in *A. thaliana* and a longer activation in *N. benthamiana (*Figure 7, right panel). This coincides with the functional FLS receptors in *A. thaliana* and *N. benthamiana*, and the functional EF-Tu receptor EFR in *A. thaliana*, thus it validates that the protoplast can respond to PAMPs and the responses observed are specific responses not due to mechanical stresses

3.4 Specificity of flg22-induced Ca^{2+} flux

To further validate the specificity of the Ca^{2+} signal by flg22 treatment, *Agrobacterium* flg22 ($flg22_{Agro}$), which is not recognized by *Arabidopsis* FLS2, was used alongside flg22. As shown in Figure 10 (right panel), the Ca^{2+} flux induced by flg22, is absent with $flg22_{Agro}$. This validates the specificity of PAMP-induced Ca^{2+} signal in the protoplasts.

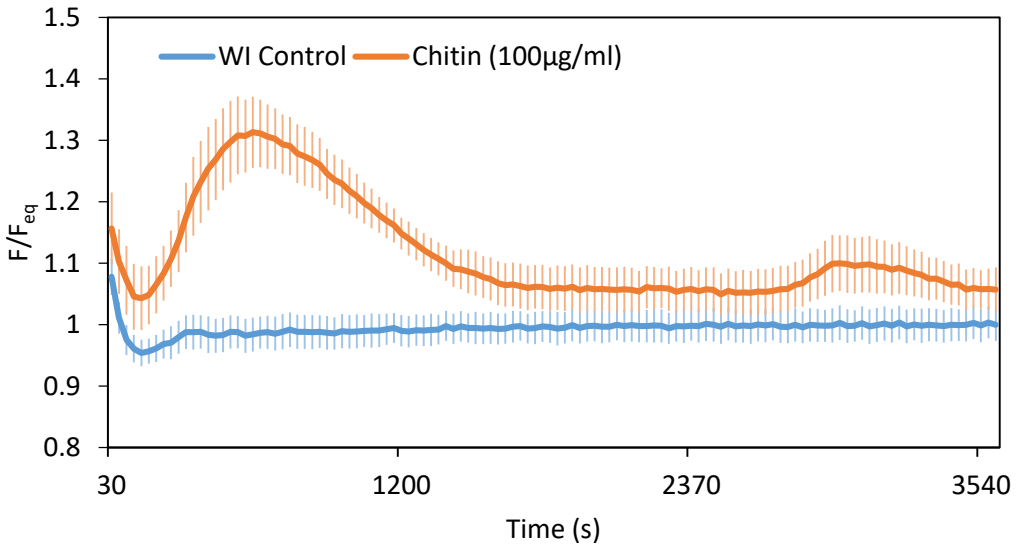

Figure 8: Fungal PAMP-induced Ca^{2+} flux in *A. thaliana* GCaMP3 protoplasts.

Protoplasts were treated with 100µg/ml chitin. WI buffer was used as a negative control (blue). n=5 and error bars represents ±SE. The experiment has been conducted at least three times with similar results.

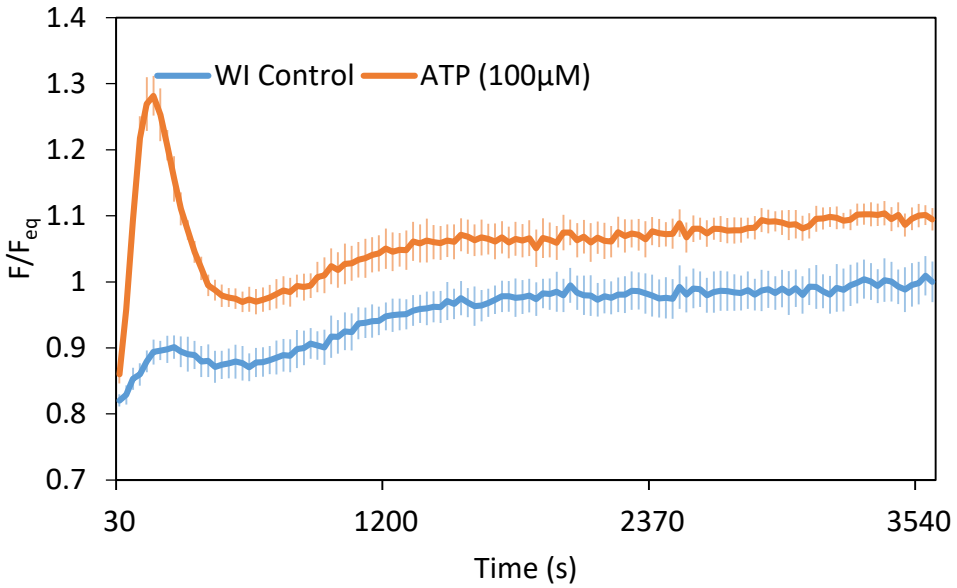

Figure 9: DAMP-induced Ca^{2+} flux in *A. thaliana* GCaMP3 protoplasts.

Protoplasts were treated with 100µM ATP. WI buffer was used as a negative control (blue). n=3 and error bars represents ±SE. The experiment has been conducted at least three times with similar results.

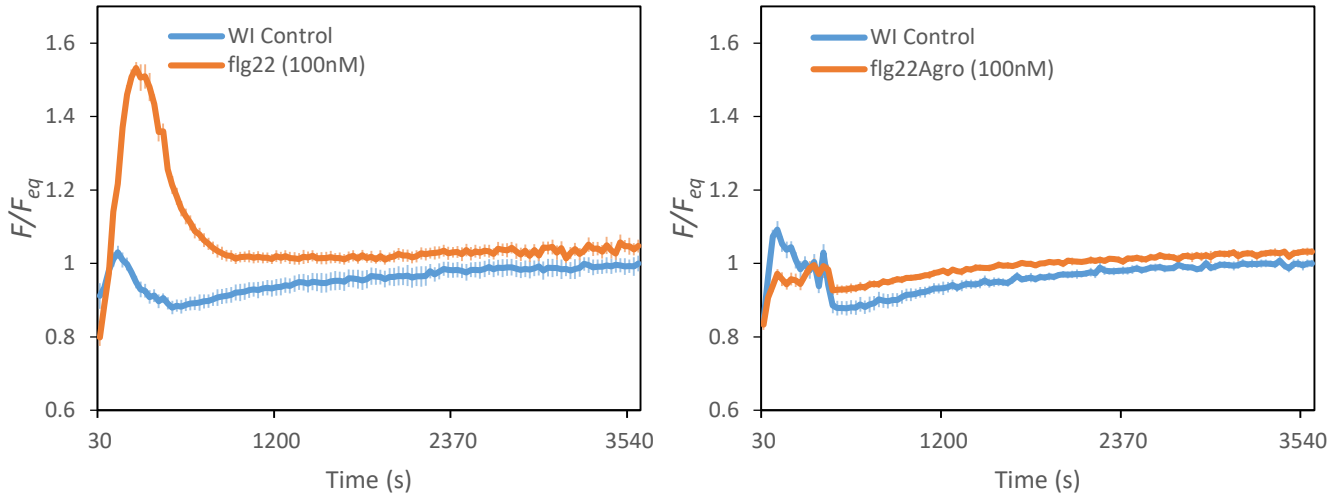

Figure 10: PAMP-triggered Ca^{2+} flux in *A. thaliana* GCaMP3 protoplasts is specific.

Protoplasts were treated with 100nM flg22 (orange, left panel) or 100nM $flg22_{Agro}$ (orange, right panel). WI buffer was used a negative control in both cases (blue). Sample size is n=5. Error bars represents ±SE. The experiment was conducted at least two times with similar results.

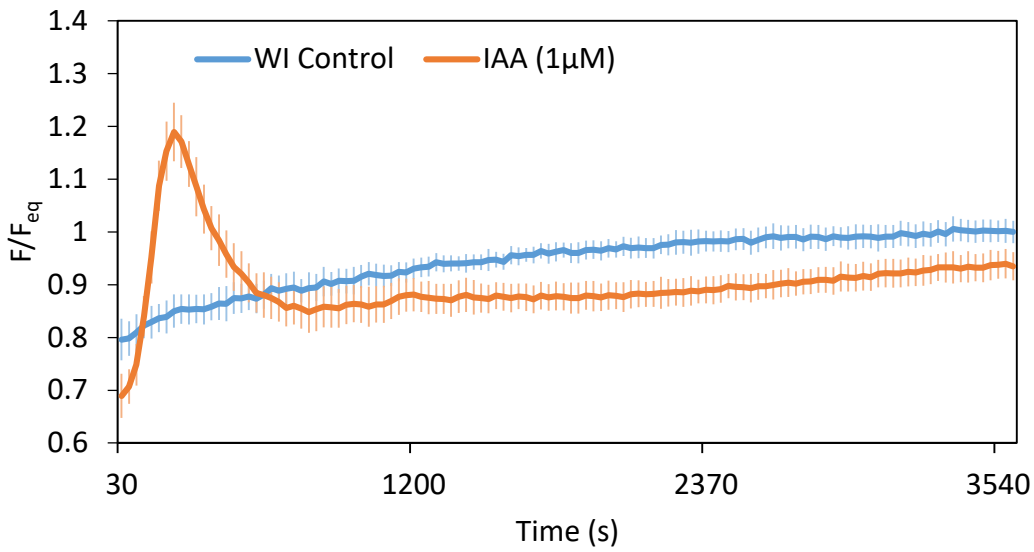

Figure 11: Hormone-induced Ca^{2+} flux in *A. thaliana* GCaMP3 protoplasts.

Protoplasts were treated with 1 µM IAA. WI buffer was used as a negative control (blue). n=3 and error bars represents ±SE. The experiment has been conducted at least three times with similar results.

3.5 Auxin-induced Ca^{2+} flux in *A. thaliana* GCaMP3 protoplasts

Auxin, a plant hormone known to be involved in plant development such as gravitropism and root hair development, has been reported to affect Ca^{2+} signaling (Shishova and Lindberg., 1999, 2004). The application of indole-3-acetic acid (IAA), which is a natural auxin, caused a rapid induction of Ca^{2+} influx with a max peak around five minutes, which declines to the resting levels around 13 min (Figure 11). This is similar to previously reported results using the synthetic auxin naphttylacetic acid (1-NAA), which increased $[Ca^{2+}]_{cyt}$ levels in protoplasts (Shishova and Lindberg., 2004; using the Furo-2 dye). This demonstrates GCaMP3 protoplasts can be used to detect hormone-induced Ca^{2+} signals in protoplasts.

3.6 Cold shock-induced Ca^{2+} flux in *N. benthamiana* GCaMP3 protoplasts

In addition to biotic stress, Ca^{2+} is known to mediate abiotic stresses, such as cold-shock. The previous Ph.D. student Dr. Thomas DeFalco has tested leaf discs from the transgenic GCaMP3 *N. benthamiana* for cold-shock induced Ca^{2+} signals. It was observed in fluorescence microscopy and quantification assays that a rapid, bi-phasic $[Ca^{2+}]_{cyt}$ elevation occurred in response to cold stress (DeFalco *et al*., 2017). Here, I tested *N. benthamiana* GCaMP3 protoplasts to evaluate if they display a similar cold stress-induced Ca^{2+} signal. I applied WI Buffer of 21°C (room temperature, control) or 4°C (cold-induced). In this assay, $[Ca^{2+}]_{cyt}$ elevation was observed at 6 min in response to cold shock, lasting for approximately 15 min (Figure 12). The timing of the cold shock-induced peak in protoplasts was similar to that of the 2^{nd} Ca^{2+} burst in leaf discs (DeFalco *et al*., 2017). Interestingly, the first rapid Ca^{2+}elevation burst was not seen the *N. benthamiana* protoplasts. *A. thaliana* protoplasts were also tested for cold shock-induced Ca^{2+} signal, however the Ca^{2+} signal occurred too quickly to be fully observed by a plate reader (data not shown). The plate reader could not capture the rise to max signal as the signal peaked quickly, only the return down to resting was observed.

3.7 Comparison of flg22-induced Ca^{2+} flux between protoplasts and leaf discs

To characterize and compare the PAMP-triggered Ca^{2+} fluxes in protoplasts and leaf discs, I used various chemical inhibitors. Protoplasts were isolated from the GCaMP3-expressing

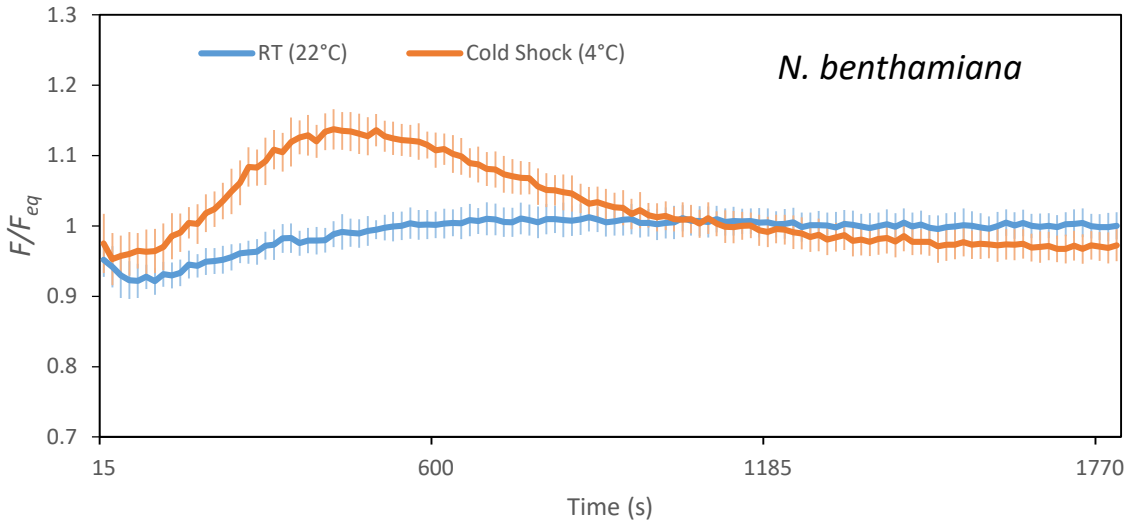

Figure 12: Cold shock-induced Ca^{2+} flux in *N. benthamiana* GCaMP3 protoplasts.

N. benthamiana protoplasts were treated with 4°C (cold shock) or 22°C (room temperature) WI buffer (control). Error bars represents ±SE. n=3. The experiment has been conducted at least two times with similar results.

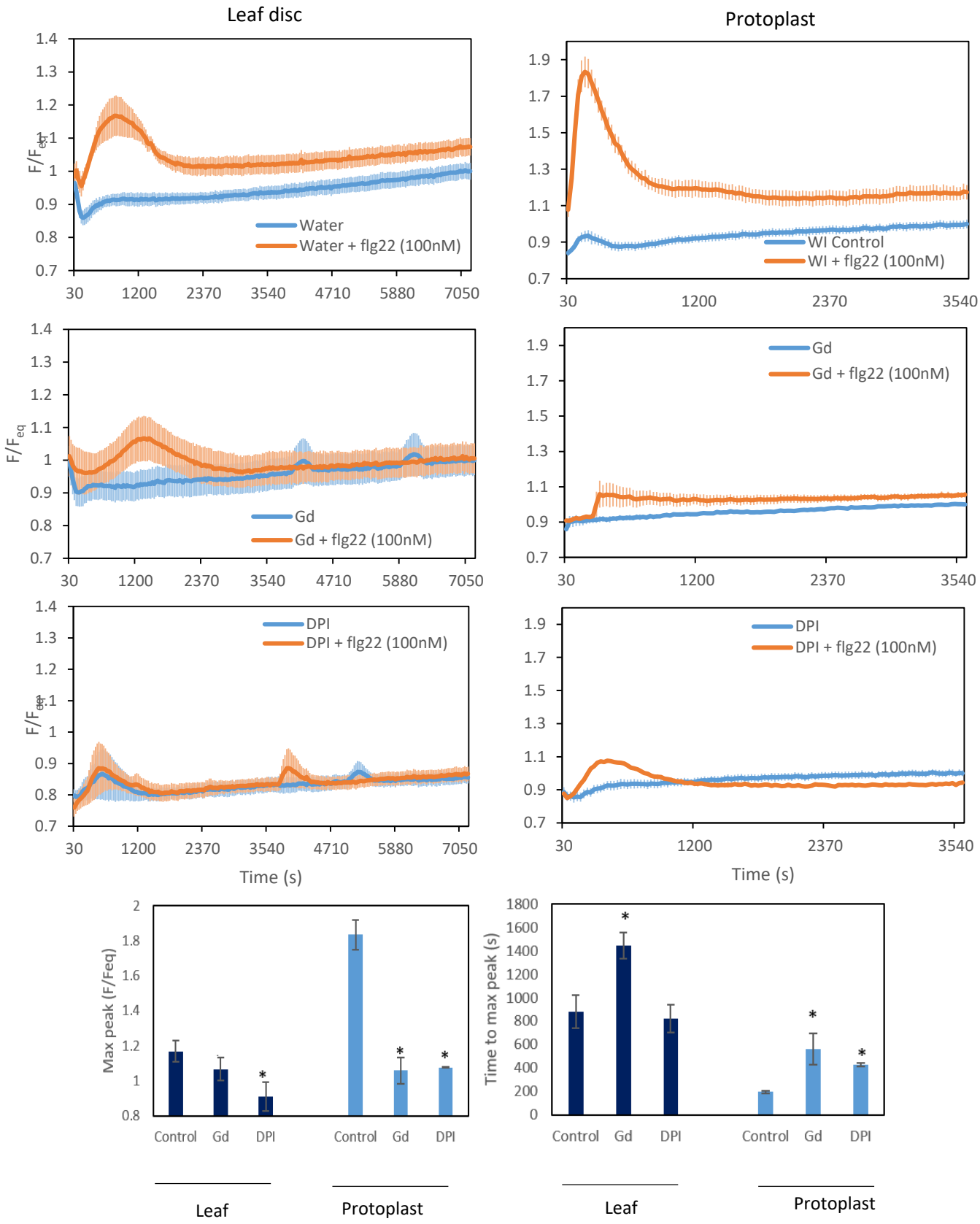

Figure 13: Effect of Gd and DPI on flg22-induced Ca^{2+} signaling in protoplasts. Leaf discs and protoplasts were equilibrated in control (water or WI buffer), Gd: gadolinium chloride, or DPI: diphenyleneidonium. Values were statistically analyzed in each group, leaf (dark blue) and protoplast (light blue). (*P<0.05, two-tailed t-test). Error bars represents ±SE. The experiment has been conducted at least three times with similar results. n=5

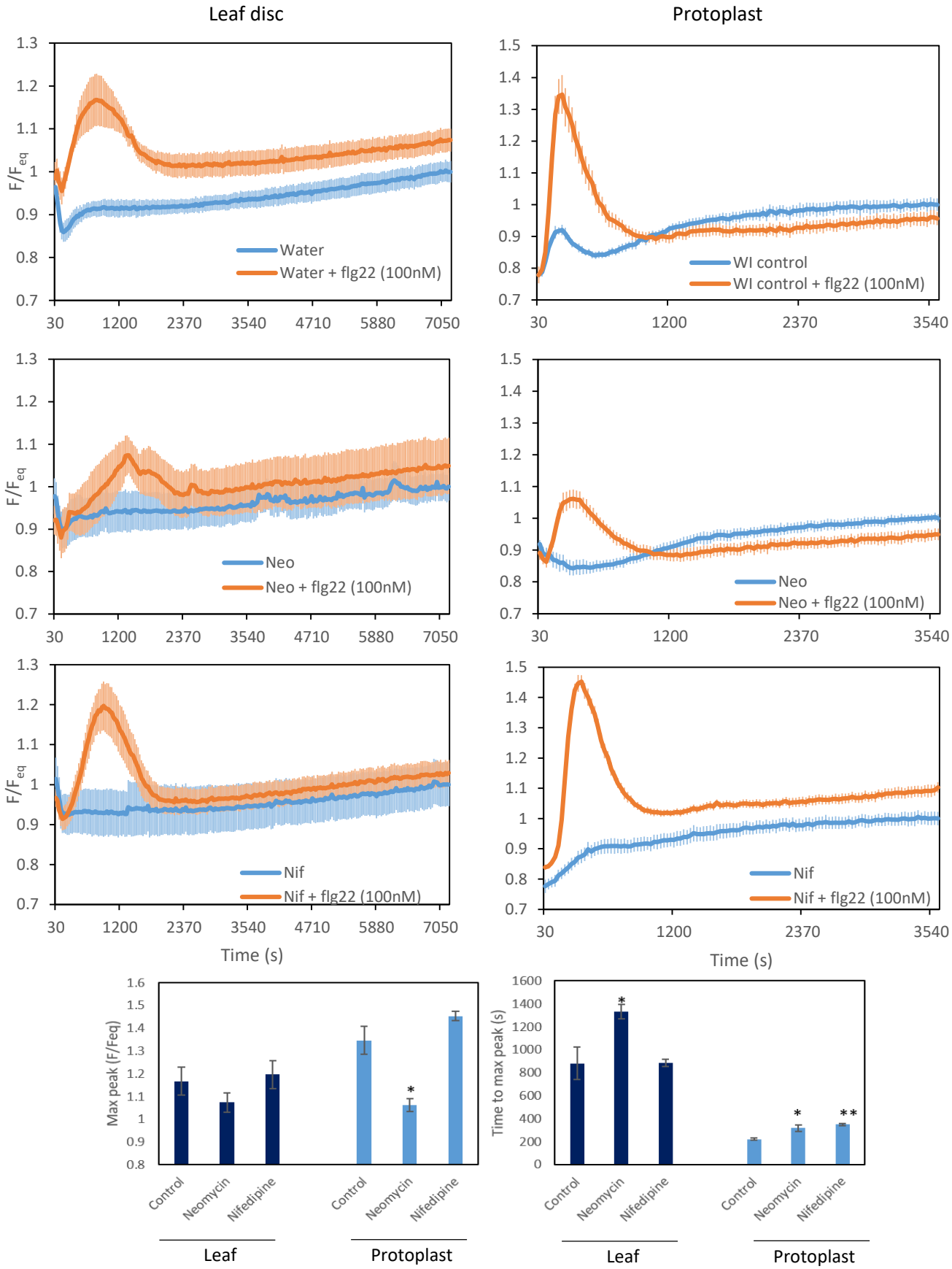

Figure 14: Effect of Neo and Nif on flg22-induced Ca^{2+} signaling in protoplasts. Leaf discs and protoplasts were equilibrated in control (water or WI buffer), Neo: neomycin, or Nif: nifedipine. Values were statistically analyzed in each group, leaf (dark blue) and protoplast (light blue). (*P<0.05 or **P<0.005, two-tailed t-test). Error bars represents ±SE. The experiment has been conducted at least three times with similar results. n=5

transgenic plants and adjusted to 2.5 x 10^5 cells/ml. 50 µl of the protoplast solution were equilibrated in 50µl of either WI buffer, or WI + inhibitor (100µM $GdCl_3$, neomycin, nifedipine, or DPI). For the leaf disc assay, 10 x 0.5cm leaf discs from 5-week old plants were equilibrated abaxial side up in 100µl of ddH_2O, or ddH_2O + inhibitors (100µM $GdCl_3$, neomycin, nifedipine, or DPI) for 2-4 hours in a Greiner 96-well flat black plate. Following equilibration, 100µl of ddH_2O (leaf disk control), WI buffer (protoplast control) or 100nM of flg22 in ddH_2O (for leaf discs) or WI buffer (for protoplasts) was added, Ca^{2+} signal was immediately measured using the plate-reader. As shown in Figure 13, pre-treatment with gadolinium (Gd^{3+}), a known Ca^{2+} channel blocker, reduced the $[Ca^{2+}]_{cyt}$ spike in both leaf discs and protoplasts in a similar manner. Pre-treatment with the NADPH oxidase inhibitor diphenyleiodonium (DPI) showed that ROS production is involved in flg22-induced Ca^{2+} signals as the Ca^{2+} signals similarly decreased with the DPI treatment (Thor and Peiter, 2014) (Figure 13).

Neomycin, a phospholipase C inhibitor which inhibits internal Ca^{2+} storage release, partially suppressed Ca^{2+} accumulation, while nifedipine, a voltage-gated channel inhibitor, did not have any observable effect on Ca^{2+} accumulation (Figure 14) (Peiter, 2011). Additionally, the decreases in max peak and time to reach to max peak with inhibitors neomycin and nifedipine are not statistically significant in leaves, but were significant in protoplasts (Figure 14). As seen in Figure 13 and 14, the peaks of Ca^{2+} signals were delayed in both leaf discs and protoplasts with these inhibitors, although only protoplasts were statistically significant. Further, without any inhibitors, the control Ca^{2+} signal peak is higher in protoplasts than that of leaf discs. In all treatments, the Ca^{2+} signals returned to the resting state in protoplasts, similar to leaf discs. Taken together, the data shows no aberrant basal Ca^{2+} signals in protoplasts but they exhibit a stronger response to the stimuli and inhibitors. This indicates that protoplasts may more readily uptake inducers and inhibitors than leaf discs. Thus, I concluded that GCaMP3-expressing protoplasts can be used to evaluate various stimuli.

3.8 Transfection of GCaMP3 into *A. thaliana* protoplasts

A published transfection protocol was tested to investigate if transiently expressed GCaMP3 can be used to evaluate Ca^{2+} signals. (Yoo *et al*., 2007). *A. thaliana* protoplasts were isolated and adjusted to two concentrations, 2.5 x 10^4 cells/100 µl or 2.5 x 10^5 cells/100 µl. Two

different amounts of GCaMP3 plasmid was tested (10 or 20µl), and either WI or W5 buffer was used as suspension and/or incubation buffer (Table 1). The transfection efficiency of each sample was determined by counting the cells with higher basal fluorescence (which can indicate successful transfection of GCaMP3) in comparison to wild-type control (Figure 15). Of the eight combinations of transfection conditions tested (Table 2), condition #8 yielded the best transfection efficiency of 81.5%. Thus, the condition #8 was used hereafter.

As shown in Figure 15, basal fluorescence of GCaMP3 can be seen in protoplasts using a microscope, indicating successful transfection. However, when I tried to quantify the signals upon flg22 treatment by the plate reader, I could not detect any increase in fluorescence (data not shown). This is likely due to not having enough healthy cells that were transfected. Thus, I have up-scaled the protoplast preparation. The original conditions used for transfection were 2.5 x 10^5 cells/100µl, 100µl of protoplasts per reaction with 10µl of 2000 ng/µl of DNA and 110µl of PEG transfection solution. These conditions were increased up to six times for one reaction. The transfected protoplasts were then incubated after transfection for 5-16 hours, where 16 hours had the best result (Figure 15).

As shown in Figure 16, the basal fluorescence levels of the transfected GCaMP3 protoplasts (orange) was significantly higher than that of the control protoplasts (blue), indicating the successful transfection. However, I still could not detect $[Ca^{2+}]_{cyt}$ increase upon flg22 treatment by the plate reader. This suggests that although I could transfect the protoplasts, it still did not reach to the threshold to be detected by the plate reader.

3.9 Detection of Ca^{2+} signals in GCaMP3 transfected *A. thaliana* protoplasts

Since the Ca^{2+} signal was not quantifiable by the plate reader, I have decided to conduct an image-based quantification. Protoplasts were prepared for 2.5x10^5 cells/100µl and then added 100nM of flg22 was added. Immediately after treatment with flg22, time-lapse images were taken every 10 seconds over 30 min. Five time points are shown in Figure 17A and the signals of four protoplasts were quantified using the Image J software, where every 10^{th} snapshot over the 30 min was quantified. Protoplasts 1 and 2 showed the basal fluorescence at time 0 indicating

Table 2: Optimizing transfection efficiency

Treatment #	*[Protoplasts per 100µL]*	*Concentration of plasmid*	*Suspension buffer*	*Incubation buffer*	*Transfection efficiency (%)*
1	2.5×10^4	1000ng/µl	WI	WI	9/80 (11.2%)
2			W5	WI	19/101 (18.8%)
3			WI	W5	3/70 (4.29%)
4			W5	W5	26/88 (29.5%)
5	2.5×10^5	2000ng/µl	WI	WI	8/95 (8.42%)
6			W5	WI	45/91 (49.5%)
7			WI	W5	5/90 (5.56%)
8			W5	W5	75/92 (81.5%)

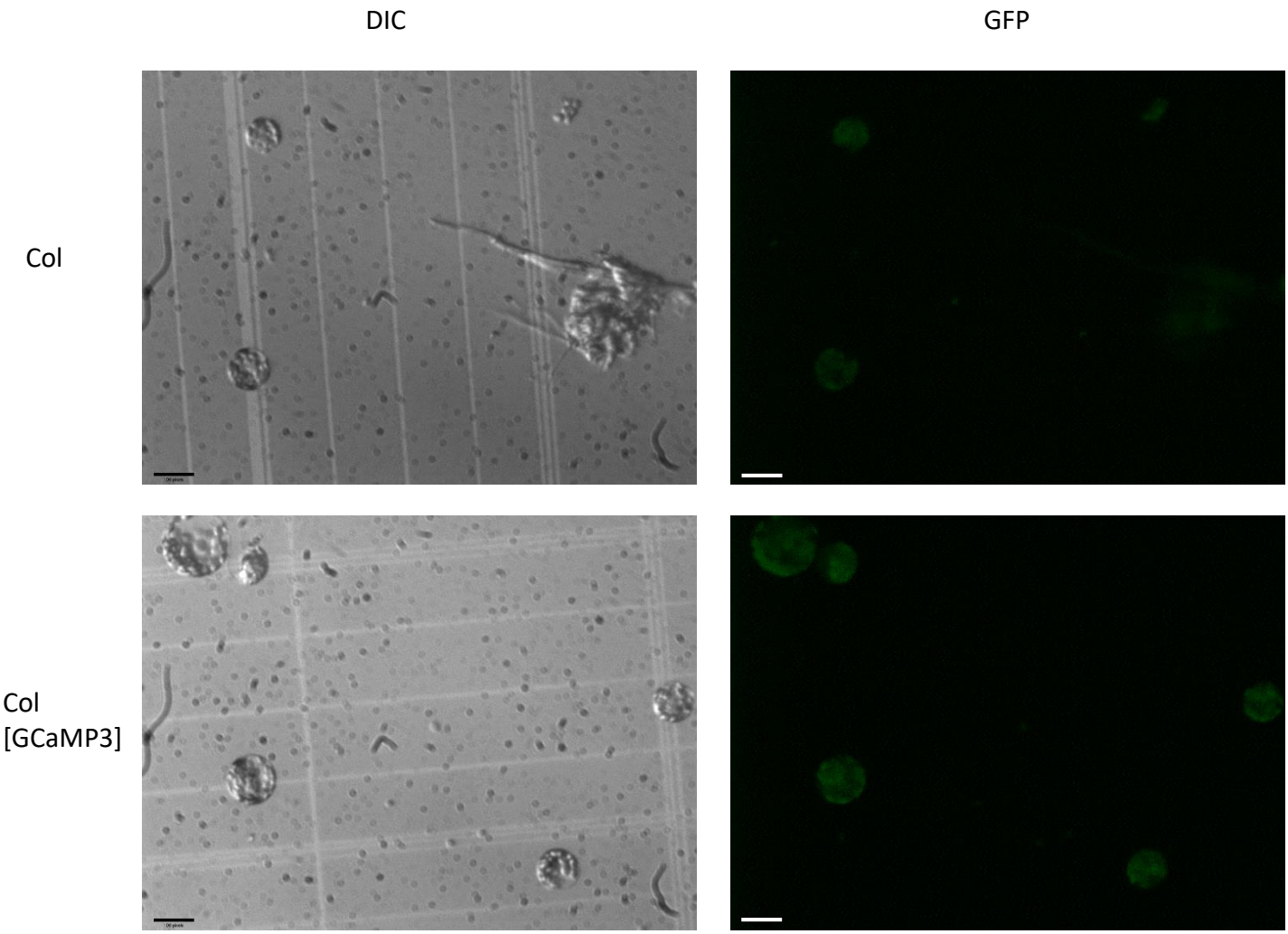

Figure 15: Basal Ca^{2+} signal activation in wild-type *A. thaliana* transfected with GCaMP3 protoplasts.
Protoplasts were transfected without plasmid (Col control) or with plasmid (Col GCaMP3) and incubated for 16 hours. Scale bar = 50 µm. The experiment was conducted at least three times with similar results. GFP image contrast were increased by 90%.

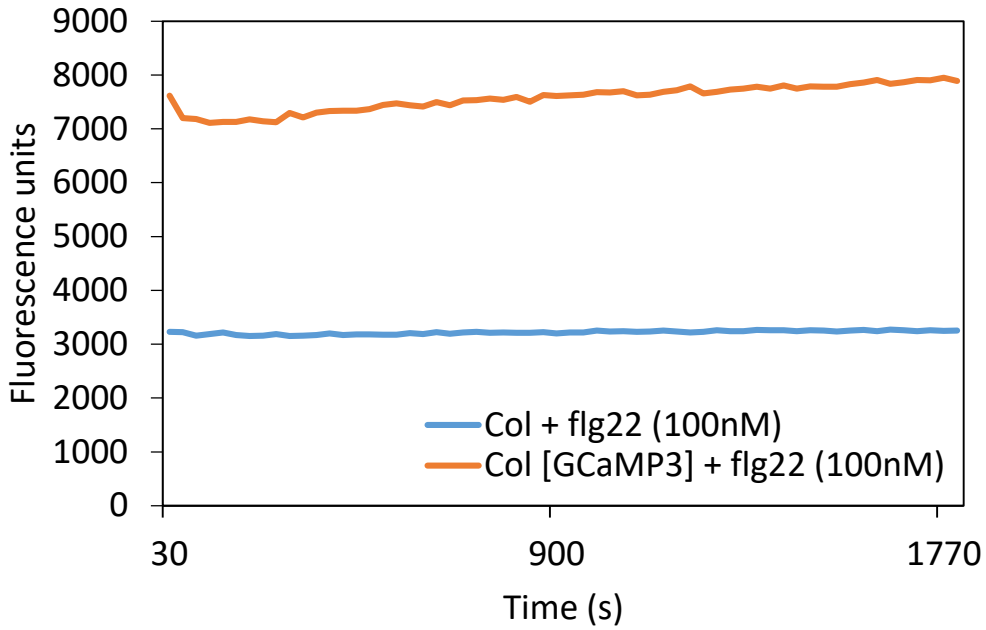

Figure 16: Transfection of GCaMP3 into protoplasts.

Wild type Col protoplasts (blue) and GCaMP3 transfected Col protoplasts (orange) were treated with 100nM of flg22. Error bars represents ±SE. The experiment was conducted at least three times with similar results.

that both were successfully transfected, whereas protoplasts 3 and 4 did not show any basal fluorescence at time 0. Thus, they were used as a control. The increase in $[Ca^{2+}]_{cyt}$ signals in two protoplasts (Protoplast 1 and 2) were observed after 8 min and went back to resting value after 30 min (Figure 17A).

The time to return to the resting value matches previously seen flg22-induced Ca^{2+} signals in protoplasts from GCaMP3 transgenic plants (Figure 7), however the initial peak in Ca^{2+} signal is delayed in comparison by two minutes. In protoplast 1 and 2, flg22-induced Ca^{2+} signal was seen with a peak of 14 and 9 fluorescence units, respectively, whereas the control protoplasts remained at 4 fluorescence units (Figure 17B). In this experiment, a total of 43 protoplasts were seen in this view and out of these only 26 showed the basal levels of fluorescence at time 0, indicating the transfection rate was about 60%. However, only 2 protoplasts (1 and 2) out of 26 responded to flg22 treatment. I have repeated similar experiments several times, but I could not see any signals like what is seen in Figure 13. Currently, the reason for unsuccessful trials is not clear.

3.10 *cpr22* has a higher basal Ca^{2+} levels than WT

As described in the introduction, *cpr22* is a rare gain-of-function mutant that is carrying the chimeric fusion of CNGCs, *AtCNGC11/12* (Yoshioka *et al*. 2006). The expression of *AtCNGC11/12* is a causal factor of *cpr22* phenotypes such as elevated levels of SA. Transient expression of *AtCNGC11/12* in *N. benthamiana* induces PCD. It is known that *cpr22*-induced cell death and homozygous lethality are Ca^{2+}-dependent (Urquhart *et al*., 2007, Abdel-Hamid *et al*., 2012). Thus, it has been hypothesized that *AtCNGC11/12* induces constitutive Ca^{2+} signals. To observe the Ca^{2+} signals in *cpr22*, GCaMP3 expressing *cpr22* line was generated by cross-pollination. These *cpr22* GCaMP3 lines and control (Ws/Col expressing GCaMP3 since c*pr22* has a Ws background and the GCaMP3 has a Col background) were analyzed using both leaf discs and protoplasts. Data in Figure 18A shows significantly higher constitutive $[Ca^{2+}]_{cyt}$ levels in *cpr22* protoplasts. Furthermore, as shown in Figure 18B, basal Ca^{2+} levels are also higher in *cpr22* leaf discs indicating the constitutive activation of Ca^{2+} signals in *cpr22*. This was predicted from a transient expression of GCaMP3 in *N. benthamiana* by Agro-infiltration (DeFalco *et al*.,

2017), however, this data is the first time to show actual elevation of Ca^{2+} signals in *cpr22* (Moeder *et al*., 2018).

3.11 Diethylstilbestrol reduces the higher constitutive Ca^{2+} levels in *cpr22*

Next, to characterize these *cpr22*-mediated Ca^{2+} signals, I have used 3 (alpha-santonin, dibucaine, and diethylstilbestrol) of 13 chemicals identified to suppress the *cpr22* phenotype from the LATCA collection (Abdel-Hamid *et al*., 2012). I have identified one chemical, diethylstilbestrol, an estrogen that impairs Ca^{2+} signals in pancreatic cells (Alonso-Magdalena *et al*., 2005) to lower the elevated $[Ca^{2+}]_{cyt}$ in *cpr22* (Figure 19). The Ws/Col leaf discs (blue) and c*pr22* leaf discs (orange) were incubated in control (water) or 100µM diethylstilbestrol for 4 hours. After 4 hour incubation, the Ca^{2+} signal was quantified using the plate reader. As seen in Figure 19, the Ws/Col leaf discs (control) did not show any difference between the control and diethylstilbestrol treatment whereas the constitutively elevated Ca^{2+} levels in *cpr22* was reduced upon diethylstilbestrol treatment. Although the decrease is not statistically significant, this experiment has been conducted several times with similar tendency.

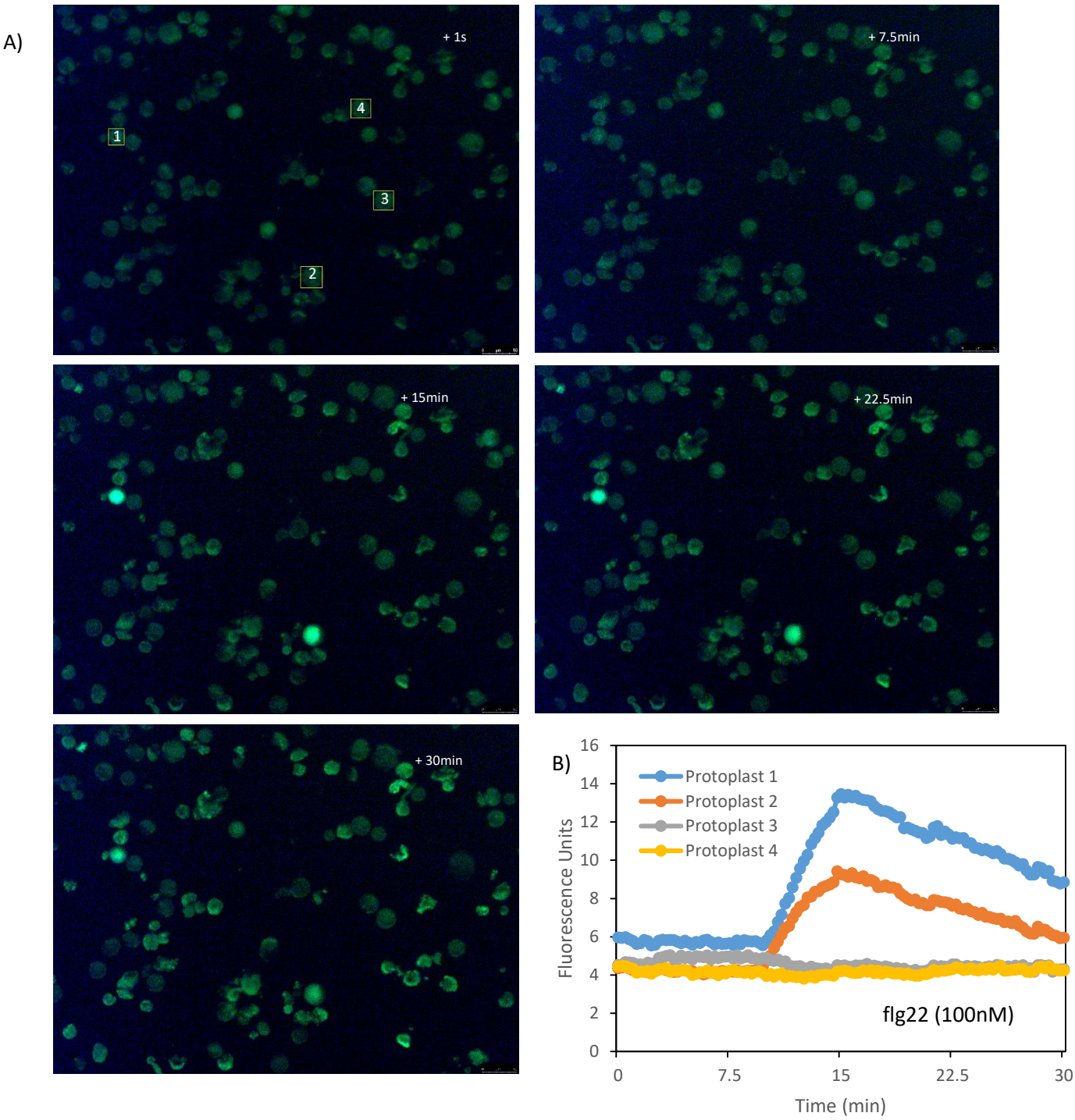

Figure 17: PAMP-triggered Ca^{2+} signal activation in transfected *A. thaliana* GCaMP3 protoplasts.

Transfected protoplasts were incubated for 16 hours followed by treatment with 100nM flg22. Images were taken every 10 s for 30 min. Images were analyzed with Image J software. Scale bar = 100µm. Image contrast was increased by 90%.

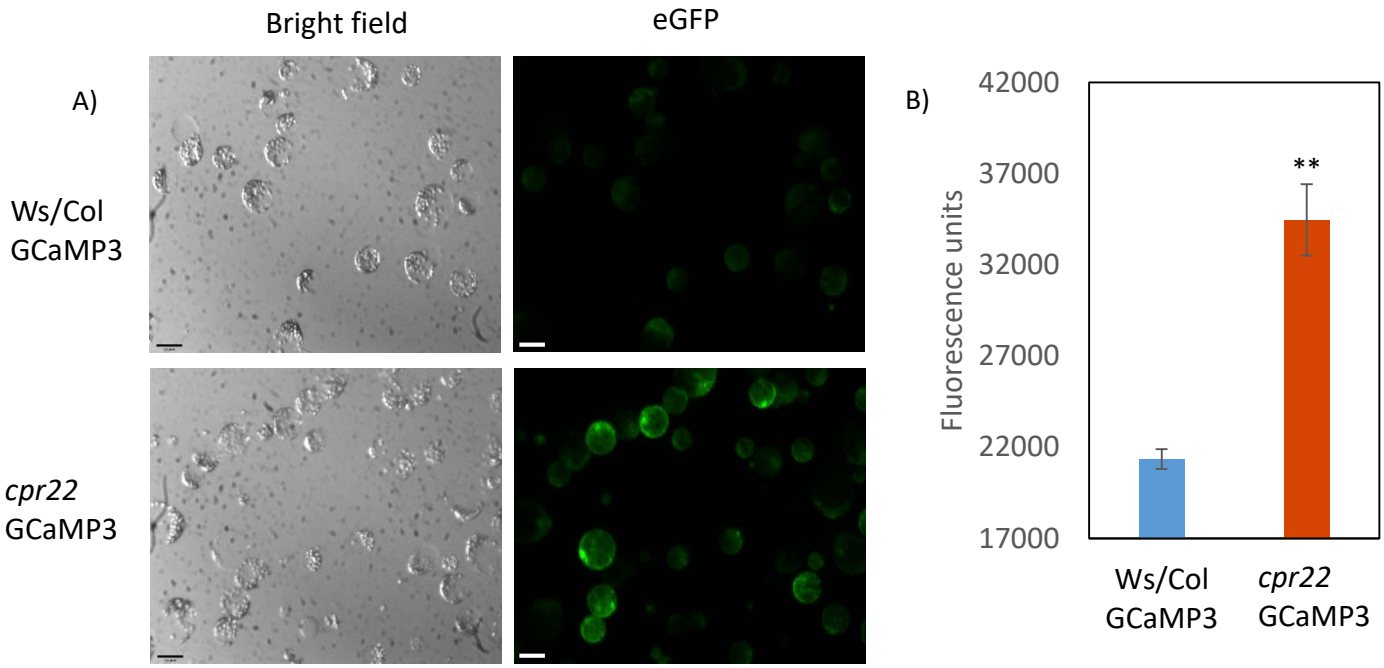

Figure 18: *cpr22* GCaMP3 protoplasts and leaf discs show higher basal Ca^{2+} signal level than wild-type.

A) Ws/Col GCaMP3 protoplasts (top row) and *cpr22* GCaMP3 protoplasts (bottom row). Scale bar = 50µm. B) Ws/Col leaf discs (blue) and *cpr22* GCaMP3 leaf discs (orange) were standardized in water for 4 hours before measurement. An average of basal level over one hour, two leaf discs/plant (**P<0.005, two-tailed t-test). n=8. Error bars show ±SE.

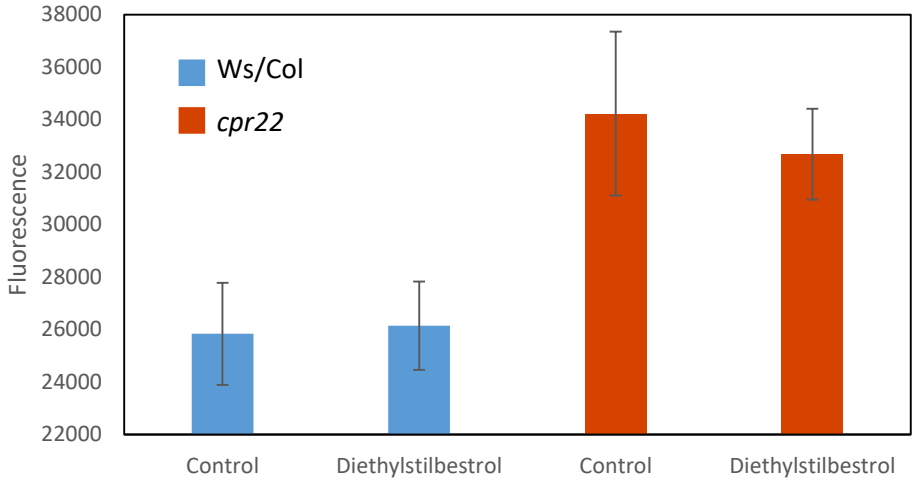

Figure 19: Diethylstilbestrol reduces the higher basal level of Ca^{2+} signaling in *cpr22*.

Ws/Col leaf discs (blue) and *cpr22* GCaMP3 leaf discs (orange) were normalized in water (control) or 100µM diethylstilbestrol for 4 hours before measurement. Error bars represent ±SE. The experiment has been conducted at least three times with similar results. n=8

Chapter 4

4 Discussion

In this study, I aimed to demonstrate the validity of using *A. thaliana* leaf mesophyll protoplasts as a tool to analyze Ca^{2+} signals using GCaMP3. Furthermore, this system can be an easy method to test various stimuli not only in *A. thaliana* but also *N. benthamiana* protoplasts (Figure 7).

Ca^{2+} is known as a universal second messenger in plants (Sanders *et al*., 2002). Previous studies using various Ca^{2+} indicators have been able to visualize and measure the transient Ca^{2+} spikes upon both biotic and abiotic stimuli (Maintz *et al*., 2014; DeFalco *et al*., 2017). GCaMP3 is advantageous among available Ca^{2+} indicators as it is not only easy to use with conventional fluorescence microscopy (Figure 5) but the fluorescence signals can also be easily quantified using a plate reader. In particular, I succeeded in capturing the Ca^{2+} responses to the bacterial elicitor, flg22 (Figure 7), the fungal elicitor, chitin (Figure 8) and a DAMP, ATP (Figure 9) with the plate reader using protoplasts. In addition, I have detected a Ca^{2+} signal after auxin treatment (Figure 10) and cold shock-induced Ca^{2+} response (Figure 11) indicating the versatility of protoplasts for a wide variety of studies. I have also validated the specificity of the flg22-induced Ca^{2+} signal using $flg22_{Agro}$, which is not recognized in *Arabidopsis* (Figure 9, Bauer *et al.*, 2001). This further indicates the ability for protoplasts to elicit a Ca^{2+} response that is not due to mechanical stress.

Protoplasts provide a relatively homogenous mixture of cells and are adjustable in concentration depending on the experiment. This minimizes the experimental variation often seen when whole seedlings or whole leaves are used. Our GCaMP3 protoplast system showed that in comparison to leaf discs, the standard error is substantially lower (Figure 9 and 10). Furthermore, a single batch of protoplasts can be used to test multiple stimuli in one experiment allowing for direct comparison.

Previous studies have shown the possibility to use shoots and roots for protoplast preparation, further showing the vast ability of this system to test various cell types (Zhai *et al*.,

2009; Bargmann and Bimbaum 2010). A protoplast system was also used as a tool to visualize Ca^{2+} response using the Ca^{2+} sensitive luminescence protein, aequorin by plasmid transfection (Maintz *et al*., 2014). It normally takes a significant amount of time to genetically introduce GECIs by cross-pollination or transformation. Protoplast transfection allows the evaluation of the effects of multiple genes of interest by transfecting GCaMP3 into mutant backgrounds. Alternatively, GCaMP3-expressing protoplasts could be transfected with gene-silencing constructs such as RNAi or CRISPR/Cas9 (Zhai *et al*., 2009; Lin *et al*., 2017). Thus, we have transfected with GCaMP3 plasmids into a wild-type Col background to transiently visualize and capture the Ca^{2+} response (Figure 15). As shown in Figure 16, the basal levels of fluorescence in the transfected protoplasts with GCaMP3 were higher than that of the un-transfected control indicating successful transfection. Next, I have tried to quantify Ca^{2+} signal activation upon stimuli in the transfected protoplasts. Based on my data using protoplasts derived from stable transgenic GCaMP3 plants, to be able to detect Ca^{2+} signals, the number of cells must be around $2.5x10^5$ per well. However, after the process of transfection, the yield of transfected protoplasts was five times less than what is needed for the plate reader usage. Thus, the failure to detect a Ca^{2+} signal in GCaMP3-transfected protoplasts by the plate reader system is probably due to the lack of enough transfected cells per well. Therefore, to have enough transfected cells for plate reader analysis, the transfection protocol had to be increased by five times from the original amount. In addition, this calculation was based on the assumption that the transfection rate is nearly 100%. The highest transfection rate achieved in this study was about 80%. Thus, to increase the transfection rate, I have changed three parameters: 1. the number of cells, 2. the amount of plasmid DNA, and 3. the incubation time after transfection. Despite a series of attempts by changing these three factors, the flg22-induced Ca^{2+} signal could not be detected by the plate reader. Further attempts of optimization to the transfection protocol are required for the use of a plate reader.

Since the flg22-induced Ca^{2+} signal response from the transfected protoplasts was undetectable by the plate-reader, I continued with the visualization of transfection under the microscope to quantify the signals. Although 26 cells of 43 were detected to have elevated basal fluorescence (successful transfection), only 2 cells showed a flg22-induced Ca^{2+} signal (Figure 17). One potential cause of this failure could be due to the treatment method of flg22. In the next

trials, flg22 was mixed into the sample beforehand to ensure even distribution, however I still did not see any signal.

I speculated that a few other underlying conditions might be responsible for the low responsiveness of the transfected protoplasts. A possible reason is that transfection protocol may cause stress to the protoplasts, thus it is probable that the protoplasts are not healthy enough to properly respond to stimuli. To validate each experiment, a positive control to flg22 treatment, consisting of transgenic GCaMP3 *A. thaliana* protoplasts that underwent the transfection protocol, was used and showed flg22-induced Ca^{2+} signals, thereby validating the success of the protocol. Older or unhealthy plants were also not ideal for making protoplasts as age and stress can compromise the protoplast transfection (Yoo *et al*., 2007). Some plants might have undergone unknown stress prior to the experiment, which in turn could have affected their response to stimuli (Knight *et al*., 1998). Finally, it is also possible that I could not detect the Ca^{2+} signals in the transfected protoplasts if the cells require more time to express the gene of interest and the time allotted in the previous trials are insufficient for the GCaMP3 expression. However, in spite of increasing incubation time to 16 hours, I could still not see any flg22-induced Ca^{2+} response in the transfected protoplasts. At this point, it is unclear what the reasons are for the low responsiveness of the transfected protoplasts. That said, once transfection of GCaMP3 in the protoplasts are perfected, it can offer the ability to test candidate genes for Ca^{2+} signaling via Ca^{2+} channels like CNGCs (Yoshioka *et al*., 2006; Urquhart *et al*., 2007).

GCaMP3 protoplasts were also used in pharmacological studies (Figure 13 and 14). Protoplasts may be a better option in comparison to leaf discs as they seem to take up chemicals more efficiently and respond in a more synchronized manner than cells in leaf discs. In these experiments, I noticed that the kinetics of the flg22-induced Ca^{2+} signals is different between protoplasts and leaf discs. The flg22-induced Ca^{2+} signals were much stronger in protoplasts than that observed in leaf discs. As shown in Figure 13 and 14, leaf discs showed about 1.2 F/F_{eq} at its peak, whereas protoplasts showed significantly more (1.7 and 1.4, respectively). These signal strengths are likely correlated to the amount of GFP proteins (thus, the number of cells), therefore the comparison of the strength may not be biologically relevant. Nevertheless, the differences in the time to reach max peak and the time to return to the resting levels must be

biologically relevant to discuss. The Ca^{2+} signal in protoplasts reached the max peak much faster. Furthermore, the duration of the Ca^{2+} signal activation was much shorter in comparison to that of leaf discs. The duration of the Ca^{2+} signal in leaf discs lasted over 1200s. However, in protoplasts, the Ca^{2+} signal returned to the almost resting levels around 900s, indicating the quick and short duration response in protoplasts. This difference in protoplasts could be due to the lack of cell wall (the absorption of flg22 is quicker), and a more synchronized response, since the population of cells is more homogenous and all the cells are receiving flg22 at the same time, while in leaf discs flg22 has to diffuse into the leaf discs. Furthermore, in leaf discs, a second wave of Ca^{2+} signals can be generated upon cell-to-cell signal activation (Gilroy *et al*., 2014). A preliminary analysis conducted by a confocal microscope captured a quick oscillation of Ca^{2+} signals in each individual cell in young seedlings after stimulation by photobleaching (data not shown). This type of oscillation could be related to cell-to-cell communication that likely does not occur in protoplasts. Thus, the leaf discs data likely include the second waves of Ca^{2+} activated by cell-to-cell communication and in contrast, the protoplasts data represent just single cell responses. However, despite these significant differences in their kinetics, fundamental responses between protoplasts and leaf discs seem to be the same and I do not see any signs of stress (i.e. by removal of cell walls)-induced aberrant Ca^{2+} signals, thus I concluded that we can use protoplasts for further experiments.

The pharmacological assay shows the Gd^{3+}, a well-known Ca^{2+} channel blocker, successfully reduced flg22-induced Ca^{2+}signals, not only in leaf discs but also in protoplasts. Interestingly, in both cases, the peaks went back to the same levels (1.1 F/F_{eq}), despite the fact that the max peaks by flg22 treatment in protoplasts were much higher. This may indicate effective suppression of signals by Gd^{3+}. This kind of observation was also seen in both leaf discs and protoplasts for a phospholipase C inhibitor, neomycin (Figure 14), where the reduction in Ca^{2+} signals support previous work that internal Ca^{2+}release plays a role to elevate Ca^{2+} upon flg22 treatment (DeFalco *et al*., 2017; Thor and Peiter, 2014). The NADPH oxidase inhibitor, DPI, did not reduce the signal in leaf discs but it did in protoplasts (Figure 13). Only a voltage-gated channel inhibitor, nifedipine, did not show any suppression in both samples and the signal could be enhanced in protoplasts (Figure 14). However, there is a slight delay in time to max peak with nifedipine treatment in protoplasts, further corroborating previous studies that

demonstrate a delay in recovery in Arabidopsis flg22-induced Ca^{2+} fluxes after the treatment with nifedipine (Kwaaitaal *et al*., 2011). Taken together, these chemical inhibitors allow us to have some insight into possible molecular components involved in generating Ca^{2+} signals upon specific triggers. Additionally, protoplasts show more effective activation and inhibition of Ca^{2+} signals, thus showing advantage in chemical uptake in protoplasts in comparison to leaf discs.

Lastly, *cpr22* has a constitutively higher Ca^{2+} signal in protoplasts, leaf discs, and detached whole leaves (Figure S1). This is the first data to directly show the elevated Ca^{2+} levels in *cpr22.* A previous Ph.D. student Dr. Huda Abdel-Hamid, conducted a chemical screen and identified 13 chemicals from the LATCA collection which suppress the *cpr22* phenotype. Of three inhibitors that were tested among these 13 (alpha-santonin, dibucaine and diethylstilbestrol), I have identified one chemical, diethylstilbestrol, which lowered the constitutive Ca^{2+} flux in *cpr22.* Diethylstilbestrol, a synthetic estrogen, has previously been used to impair Ca^{2+} signals in pancreatic cells in mice (Alonso-Magdalena *et al*., 2005). Other recent study has been implicated diethylstilbestrol to be involved in the phospholipase C (PLC) and cyclic adenosine monophosphate (cAMP) –response element binding protein pathway (CREB) in mice testis cells (Zhang *et al*., 2012, 2014, 2015, 2018). These studies provide evidence for diethylstilbestrol's potential molecular mechanism. Currently, no reports have investigated the effect of diethylstilbestrol in plants. The future tests of diethylstilbestrol, PLC inhibitors (such as neomycin) and cAMP in *A. thaliana* could yield interesting results. Through the use of the *cpr22* GCaMP3 line, we can further examine the role of not only diethylstilbestrol, but also other chemicals that could reduce a high basal Ca^{2+} level, and dissect CNGC-mediated Ca^{2+} signal pathway.

Overall, the combination of protoplasts and GCaMP3 can be a great tool to use to analyze Ca^{2+} responses in not only wild-type but various mutants by transient expression of GCaMP3. This GCaMP3 protoplast system is advantageous to other systems for various reasons: an easier uptake of inducers and inhibitors due to lack of cell wall, a faster response, and a large number of genes of interest can be studied using transfection in a shorter duration. My thesis project evaluated the basics of Ca^{2+} signals captured by GCaMP3 in protoplasts and concluded that with further optimization of the protocol, protoplasts can use used for future analysis.

References

Abdel-Hamid H, Chin K, Moeder W, and Yoshioka K. 2011. High throughput chemical screening supports the involvement of Ca^{2+} in cyclic nucleotide-gated ion channel-mediated programmed cell death in Arabidopsis. Plant Signal Behav. 6: 1817–1819.

Albert M. 2013. Peptides as triggers of plant defense. J Exp Bot. 64: 5269-5279.

Alonso-Magdalena P, Laribi O, Ropero A, Fuentes E, Ripoll C, Sora B, Nadal A. 2005. Low doses of bisphenol A and diethylstilbestrol impair Ca2+ signals in pancreatic α-cells through a nonclassical membrane estrogen receptor within intact islets of Langerhans. Environ Health Persp.113: 969-977.

Asai T, Stone JM, Heard JE, Kovtun Y, Yorgey P, Sheen J, Ausubel FM. 2000. Fumonsin B1-induced cell death in Arabidopsis protoplasts requires jamonate-,ethylene-, and salicyclic-dependent signaling pathways. Plant Cell. 12: 1823-1836.

Batistič O, Kudla J. 2012. Analysis of calcium signaling pathways in plants. Biochimica Biophys Acta. 1820: 1283–1293.

Bauer Z, Gomez-Gomez L, Boller T, Felix G. 2001. Sensitivity of different ecotypes and mutants of Arabidopsis thaliana toward bacterial elicitor flagellin correlates with the presence of receptor-binding sites. J Biol Chem. 276: 45669-45676.

Bektas Y, Eulgem T. 2015. Synthetic plant defense elicitors. Front Plant Sci. 5: 804.

Berridge MJ, Bootman MD, Roderick HL. 2003. Calcium signaling: dynamics, homeostasis and remodeling. Nat Rev Mol Cell Bio. 4: 517-529.

Brunner F, Rosahl S, Lee J, Rudd J, Geiler C, Kauppinen S, Rasmussen G, Scheel D, Nürnberger T. 2002. Pep-13, a plant defense-inducing pathogen-associated pattern from Phytophthora transglutaminases. EMBO J. 21: 6681-6688.

Cao Y, Liang Y, Tanaka K, Nguyen C, Jedrzejczak R, Joachimiak A, and Stacey G. 2014. The kinase LYK5 is a major chitin receptor in Arabidopsis and forms a chitin-induced complex with related kinase. Elife. 3: e03766.

Carafoli E. 2003. The calcium-signaling saga: tap water and protein crystals. Nat Rev Mol Cell Biol. 4: 326-332.

Chandra S, Low PS. 1997. Measurement of Ca2+ fluxes during elicitation of the oxidative burst in aequorin-transformed tobacco cells. J Biol Chem. 272: 28274–28280.

Clapham D. 2007. Calcium signaling. Cell. 131: 1047–1058.

Coll N, Epple P, Dangl J. 2011. Programmed cell death in the plant immune system. Cell Death Differ. 18: 1247–1256.

DeFalco TA, Bender K, Snedden W. 2010. Breaking the code: Ca2+ sensors in plant signaling. Biochemical J. 425: 27–40

DeFalco TA, Toyota M, Phan V, Karia P, Moeder W, Gilroy S, Yoshioka K. 2017. Using GCaMP3 to study Ca2+ signaling In *Nicotiana* species. Plant Cell Physiol. 0: 1-12.

Demidchik V, Essah P, Tester M. 2004. Glutamate activates cation currents in the plasma membrane of Arabidopsis root cells. Planta. 219: 167-175.

Edel KH, Kudla J. 2015. Increasing complexity and versatility: How the calcium signaling toolkit was shaped during plant land colonization. Cell Calcium. 75: 231-246.

Forde G, Cutler S, Zaman N, Krysan P. 2013. Glutamate signaling via MEKK1 kinase-dependent pathway induces changes in Arabidopsis root architecture. Plant J. 75: 1-10.

Gilroy S, Suzuki N, Miller G, Choi WG, Toyota M, Devireddy AR, Mittler R. 2014. A tidal wave of signals: calcium and ROS at the forefront of rapid systemic signaling. Trends Plant Sci. 19: 623-630.

Horikawa K, Yamada Y, Matsuda T, Kobayashi K, Hashimoto M, Matsu-ura T, Miyawaki A, Michikawa T, Mikoshiba K, Nagai T. 2010. Spontaneous network activity visualized by ultrasensitive Ca^{2+} indicators, yellow Cameleon-Nano. Nat Methods. 9: 729-732.

Jones JDG, Dangl L. 2006. The plant immune system. Nature. 444: 323–329.

Kaplan B, Sherman T, Fromm H. 2007. Cyclic nucleotide-gated channels in plants. FEBS Lett. 581: 2237–2246.

Kaupp UB, Seifert R. 2002. Cyclic nucleotide-gated ion channels. Physiol Rev. 82: 769-824.

Klüsener B, Boheim G, Liss H, Engelberth J, Weiler E. 1995. Gadolinium-sensitive, voltage-dependent calcium release channel in endoplasmic reticulum of a higher plant mechanoreceptor organ. EMBO J. 14: 2708-2714.

Knight H, Brandt S, Knight M. 1998. A history of stress alters drought calcium signaling pathways in Arabidopsis. Plant J. 16: 681-687.

Knight H, Knight M. 1995. Recombinant aequorin methods for intracellular calcium measurement in plants. Methods Cell Biol. 49: 201-216.

Knight M, Read N, Campbell A, Trewavas A. 1993. Imaging calcium dynamics in living plants using semi-synthetic recombinant aequorins. J Cell Biol. 121: 83–90.

Kunze G, Zipfel C, Robatzek S, Niehaus K, Boller T, Felix G. 2004. The N terminus of bacterial elongation factor Tu elicits innate immunity in Arabidopsis plants. Plant Cell. 16: 3496-3507.

Kwaaitaal M, Huisman R, Maintz J, Reinstadler A, Panstruga R, Reinstädler A, Panstruga R. 2011. Ionotropic glutamate receptor (iGluR)-like channels mediate MAMP-induced calcium influx in Arabidopsis thaliana. Biochem J. 440: 355-365.

Lecourieux D. 2002. Analysis and Effects of Cytosolic Free Calcium Increases in Response to Elicitors in Nicotiana plumbaginifolia Cells. Plant Cell. 14: 2627–2641.

Liang Y, Toth K, Cao Y, Tanaka K, Espinoza C, Stacey G. 2014. Lipochitoloigosaccharide recognition: an ancient story. New Phytol. 204: 289-286.

Lin CS, Hsu, CT, Yang LH, Lee LY, Fu JY, Cheng QW, Wu FH, Hsiao HC, Zhang Y, Zhang R, Chang WJ, Yu CT, Wang W, Liao LJ, Gelvin SB, Shih MC. 2017. Application of protoplast technology to CRISPR/Cas9 mutagenesis: from single-cell mutation detection to mutant plant regeneration. Plant Biotechnol J. doi: 10.1111/pbi.12870

Lindenberg L., Merkx M. 2014. Engineering Genetically Encded FRET Sensors. Sensors. 14: 11691-11713.

Loebenstein G. 2009. Local Lesions and Induced Resistance. Adv Virus Res. 75: 73-117.

Mantulef L, Zagotta WN. 2003. Cyclic nucleotide-gated ion channels. Annu Rev Cell Dev Bi. 19: 23-44.

Mäser P, Thomine S, Schroeder JI, Ward JM, Hirschi K, Sze H, Talke IN, Amtmann A, Maathuis FJ, Sanders D, Harper JF, Tchieu J, Gribskov M, Persans MW, Salt DE, Kim SA, Guerinot ML. 2001. Phylogenetic relationships within cation transporter families of Arabidopsis. Plant Physiol. 126: 1646-1667.

Maintz J, Cavdar M, Tamborski J, Kwaaitaal M, Huisman R, Meesters C, Kombrink E, Panstruga R. 2014. Comparative analysis of MAMP-induced calcium influx in Arabidopsis seedlings and protoplasts. Plant Cell Physiol. 55: 1813–1825.

Moeder W, Phan V, Yoshioka K. 2018. Ca^{2+} to the rescue – Ca^{2+} channels and signaling in plant immunity. Plant Sci. doi: 10.1016/j.plantsci.2018.04.012

Monshausen GB. 2012. Visualizing Ca2+ signatures in plants. Curr Opin in Plant Biol. 15: 677–682.

Nakai J, Ohkura M, Imoto K. 2001. A high signal-to-noise Ca(2+) probe composed of a single green fluorescent protein. Nat Biotechnol. 19: 137–141.

Peiter E. 2011. The plant vacoule: Emitter and receiver of calcium signal. Cell Calcium. 50: 120-128.

Ranf S, Eschen-Lippold L, Pecher P, Lee J, Scheel D. 2011. Interplay between calcium signaling and early signaling elements during defense responses to microbe- or damage-associated molecular patterns. Plant J. 68: 100-113.

Ranf S, Wünnenberg P, Lee J, Becker D, Dunkel M, Hedrich R, Scheel D, Dietrich P. 2008. Loss of the vacuolar cation channel, AtTPC1, does not impair Ca2+ signals induced by abiotic and biotic stresses. Plant J. 53: 287–299.

Sanders D, Pelloux J, Brownlee C, Harper JF. 2002. Calcium at the Crossroads of Signaling. Plant Cell. 14: 401–418.

Schuurink RC, Shartzer SF, Fath A, Jones RL. 1998. Characterization of a calmodulin-binding transporter from the plasma membrane of barley aleurone. P Natl Acad Sci USA. 109: 3558-3563.

Seybold H, Trempel F, Ranf S, Scheel D, Romeis T, Lee J. 2014. Ca2+ signaling in plant immune response: from pattern recognition receptors to Ca2+ decoding mechanisms. New Phytol. 204: 782–790.

Shani E, Salehin M, Zhang Y, Sanchez S, Doherty C, Wang R, Mangado C, Song L, Tal I, Pisanty O, Ecker J, Kay S, Pruneda-Paz J, Estelle M. 2017. Plant stress tolerance requires auxin-sensitive Aux/IAA transcriptional responses. Curr Biol. 27: 437-444.

Sheen J. 2001. Signal transduction in Maize and Arabidopsis Mesophyll Protoplasts. Plant Physiol. 127: 1466-1475.

Stael S., Kmiecik P., Willems P., Van Der Kelen K., Coll NS., Teige M., VanBreusegem F. 2015. Plant innate immunity—sunny side up? Trends Plant Sci. 20: 3-11.

Stone J, Heard J, Asai T, Ausubel F. 2000. Simulation of fungal-mediated cell death by fumonisin B1 and selection of fumonisin B1-resistant Arabidopsis Mutants. Plant Cell. 12: 1811-1822.

Strotmann R, Schultz G, Plant T. 2003. Ca^{2+} - dependent potentiation of the nonselective cation channel TRPV4 is mediated by a C-terminal calmodulin binding site. J Biol Chem. 18: 26541-26549.

Tanaka K, Choi J, Cao Y, Stacey G. 2014. Extracellular ATP acts as a damage-associated molecular pattern (DAMP) signal in plants. Front Plant Sci. 5: 446.

Thor K, Peiter E. 2014. Cytosolic calcium signals elicited by the pathogen-associated molecular patterns flg22 in stomatal guard cells are of an oscillatory nature. New Phytol. 4: 873-81.

Urquhart W, Gunawardena AH, Moeder W, Ali R, Berkowitz GA, Yoshioka K. 2007. The chimeric cyclic nucleotide-gated ion channel ATCNGC11/12 constitutively induces programmed cell death in a Ca2+ dependent manner. Plant Mol Biol. 65: 747-761.

Urquhart W, Chin K, Ung H, Moeder W, and Yoshioka K. 2011. The cyclic nucleotide-gated channels AtCNGC11 and 12 are involved in multiple Ca^{2+}-dependent physiological responses and act in a synergistic manner. J Exp Bot. 62: 3671-3682.

Wang H, Li J, Bostock RM, Gilchrist DG. 1996. Apoptosis: A functional paradigm for programmed plant cell death induced by a host-selective phytotoxin and invoked during development. Plant Cell. 8: 375-391.

Whitaker M. 2012. Genetically-encoded probes for measurement of intracellular calcium. Methods Cell Biol. 99:153-182.

White P, Bowen H, Demidchik V, Nichols C, Davies J. 2002. Genes for calcium-permeable channels in the plasma membrane of root cells. Biochim Biophys Acta. 1564: 299-309.

Yamada K, Yamaguchi K, Shirakawa T, Nakagami H, Mine A, Ishikawa K, Fujiwara M, Narusaka M, Narusaka Y, Ichimura K, Kobayashi Y, Matsui H, Nomura Y, Nomoto M, Tada Y, Fukao Y, Fukamizo T, Tsuda K, Shirasu K, Shibuya N, Kawasaki T. 2016. The Arabidopsis CERK1-associated kinase PBL27 connects chitin perception to MAPK activation. EMBO J. 35: 2468-2483.

Yamazaki T, Kawamura Y, Uemura M. 2009. Extracellular freezing-induced mechanical stress and surface area regulation on the plasma membrane in cold-acclimated plant cells. Plant Signal Behav. 4: 231-233.

Yoshioka K, Moeder W, Kang H, Kachroo P, Masmoudi K, Berkowitz G, Klessig D. 2006. The chimeric Arabidopsis CYCLIC NUCLEOTIDE-GATED ION CHANNEL11/12 activates multiple pathogen resistance responses. Plant Cell. 18: 747-763.

Yoo SD, Cho YH, Sheen J. 2007. *Arabidopsis* mesophyll protoplasts: A versatile cell system for transient gene expression analysis. Nat Protoc. 2: 1565-1575.

Yu IC, Parker J, Bent AF. 1998. Gene-for-gene disease resistance without the hypersensitive response in Arabidopsis *dnd1* mutant. Proc Natl Acad Sci USA. 95: 7819-7824.

Zagotta WN, Olivier NB, Black KD, Young EC, Olson R, Gouaux E. 2003. Structural basis for modulation and agonist specificity of HCN pacemaker channels. Nature. 425: 200-205.

Zhai Z, Sooksa-nguan T, Vatamaniuk OK. 2009. Establishing RNA interference as a reverse-genetic approach for gene functional analysis in protoplasts. Plant Physiol. 149: 642-52.

Zhang X, Li JH, Ma L, Huang TH, Jiang XW. 2012. Diethylstilbestrol impairs the morphology and function of mouse gubernaculum testis in culture. Cell Biol Toxicol. 28: 397-407.

Zhang X, Li JH, Duan SX, Lin QJ, Ke S, Ma L, Huang TH, Jiang XW. 2014. G protein -coupled estrogen receptor-protein kinase A-ERK-CREB signaling pathway is involved in the regulation of mouse gubernaculum testis cells by diethylstilbestrol. Arch Environ Con Tox. 67: 97-103.

Zhang X, Ke S, Chen KH, Li JH, Ma L, Jiang XW. 2015. Diethylstilbestrol affects the expression of GPER in the gubernaculum testis. Int J Clin Exp Patho. 8:7217-7222.

Zhang X, Ping HY, Li JH, Duan SX, Jiang XW. 2018. Diethylstilbestrol regulates mouse gubernaculum testis cell proliferation via PLC-Ca^{2++} -CREB pathway. Cell Biochem Funct. 36: 13-17.

Zipfel C. 2008. Pattern-recognition receptors in plant innate immunity. Curr Opin Immunol. 20: 10–16.

Supplemental Data

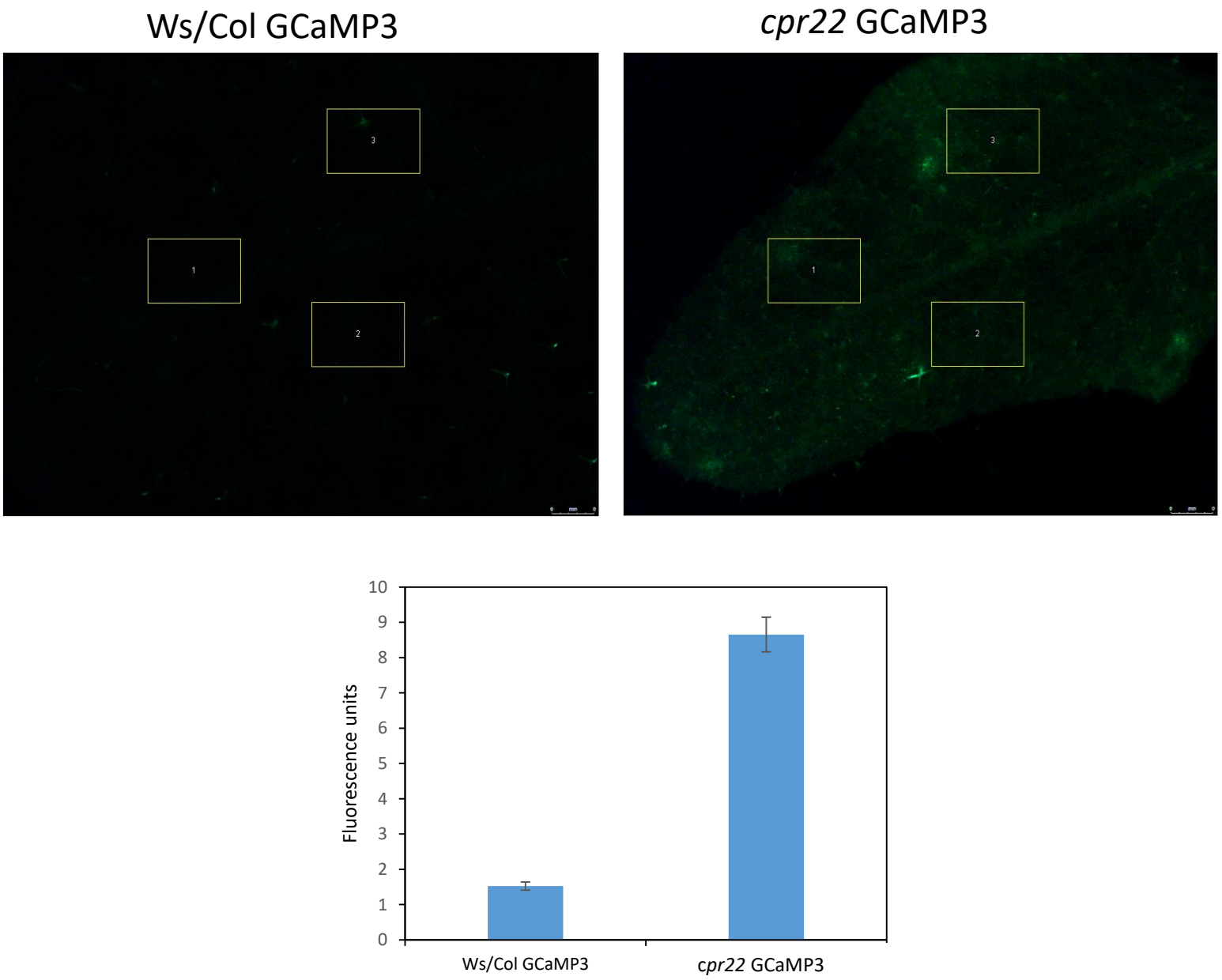

Figure S1: *cpr22* GCaMP3 leaves show a higher basal Ca^{2+} level than wild-type.

Ws/Col GCaMP3 whole leaves and *cpr22* GCaMP3 whole leaves were normalized abaxial side down for 3 hours. Scale bar = 1mm. Graph is an average of three ROI (Regions Of Interest). Error bars represents ±SE. Experiment has been repeated twice. Image contrast increased by 60%.

Appendix 1

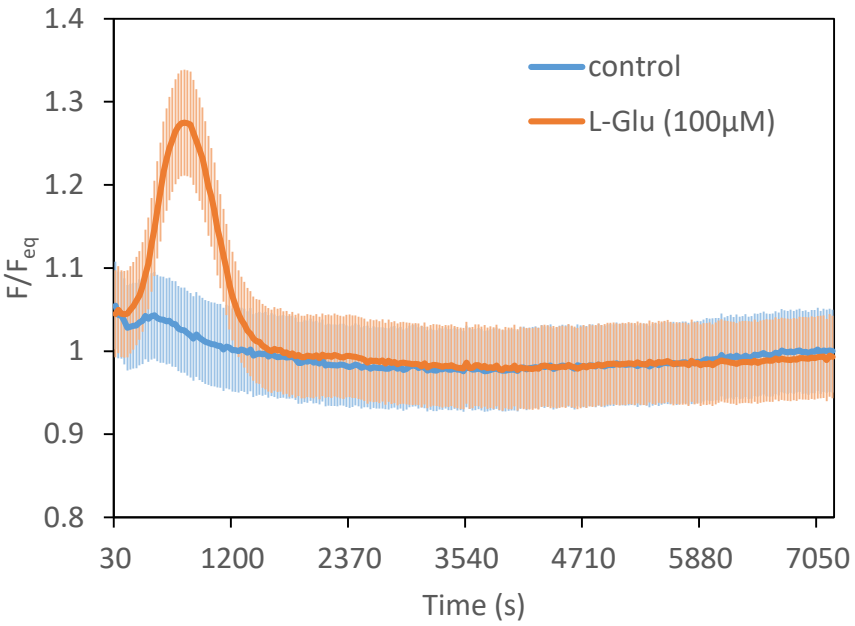

Figure A1.1: DAMP-induced Ca^{2+} flux in *N. benthamiana* leaf discs.

Leaf discs were treated with water, or 100µM L-Glu. n=5 and error bars represents ±SE. The experiment has been conducted at least three times with similar results.

Appendix 2

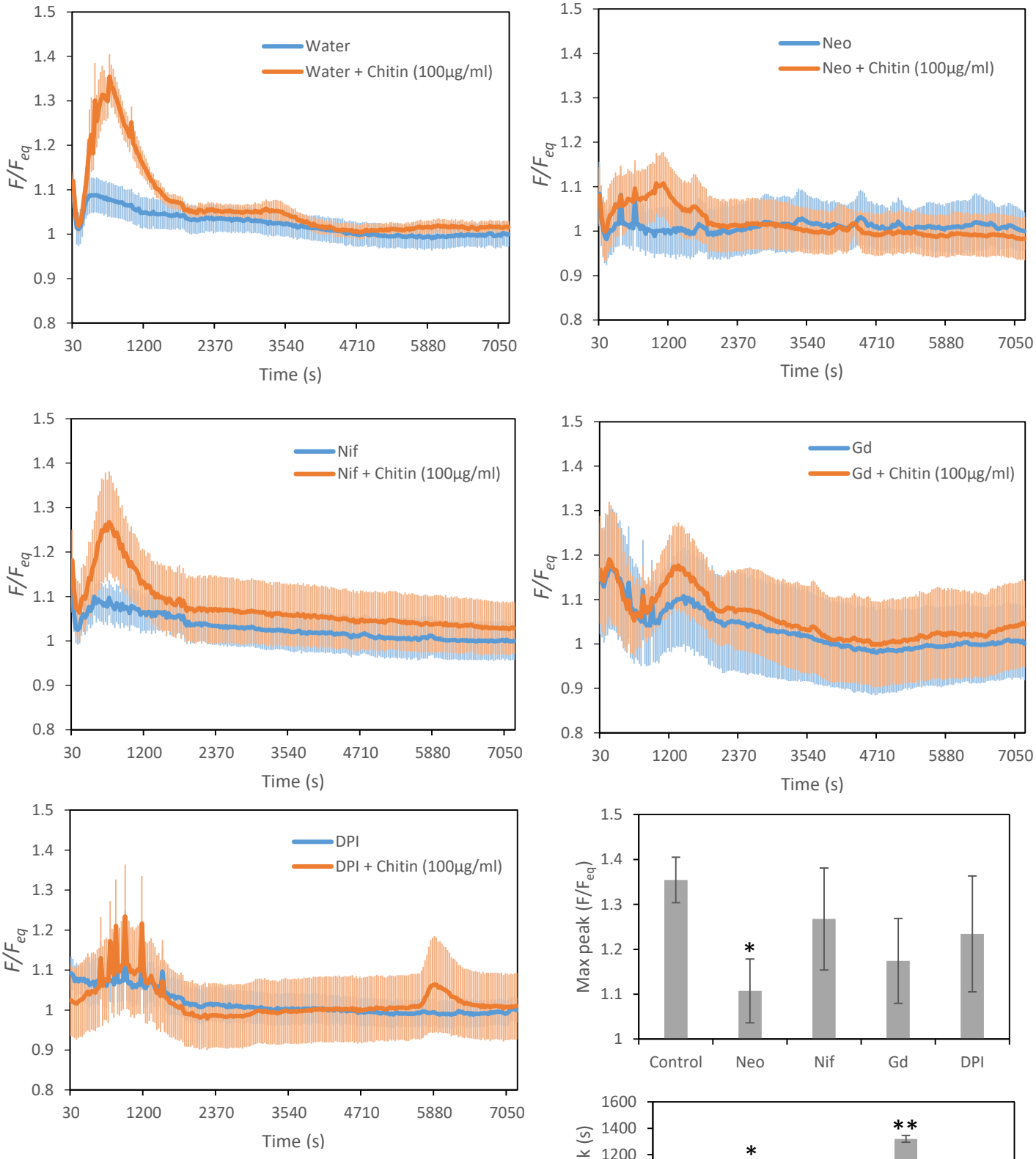

Figure A2.1: Internal Ca^{2+} release is involved in chitin-induced Ca^{2+} signals in *A. thaliana* leaf discs. Values were statistically analyzed in each group, leaf (dark blue) and protoplast (light blue). (*P<0.05 or **P<0.005, two-tailed t-test). n=5. Error bars represents ±SE. This experiment has been conducted multiple times with inconsistent results due to chitin oligomer mixture.

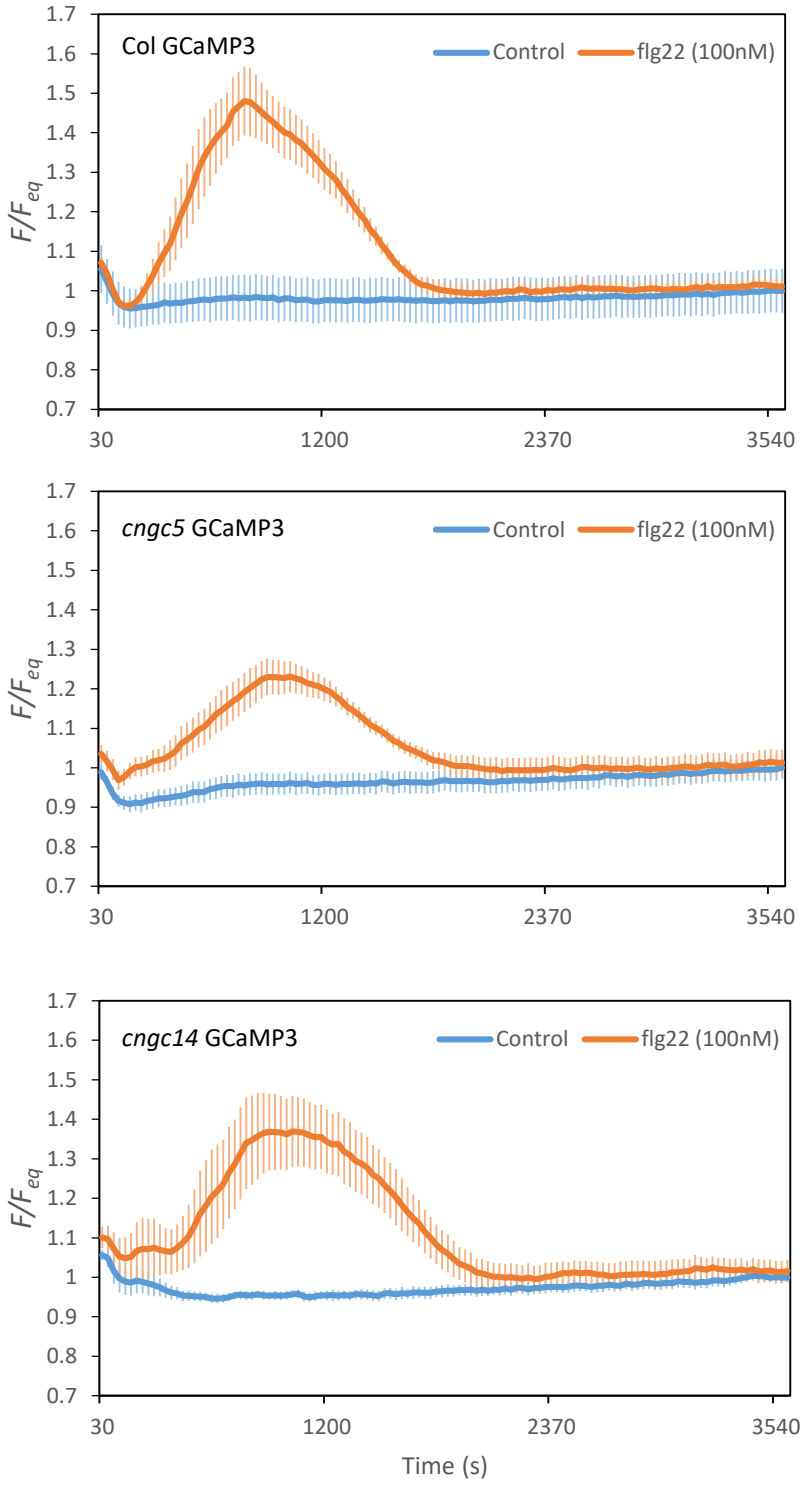

Figure A2.2: *CNGC5* may be involved in PAMP-induced Ca^{2+} response. Homozygous *cngc5* GCaMP3 and *cngc14* GCaMP3 were induced with WI control (blue) or 100nM flg22. n=5. Error bars represent ±SE. Trial was done twice with similar results.

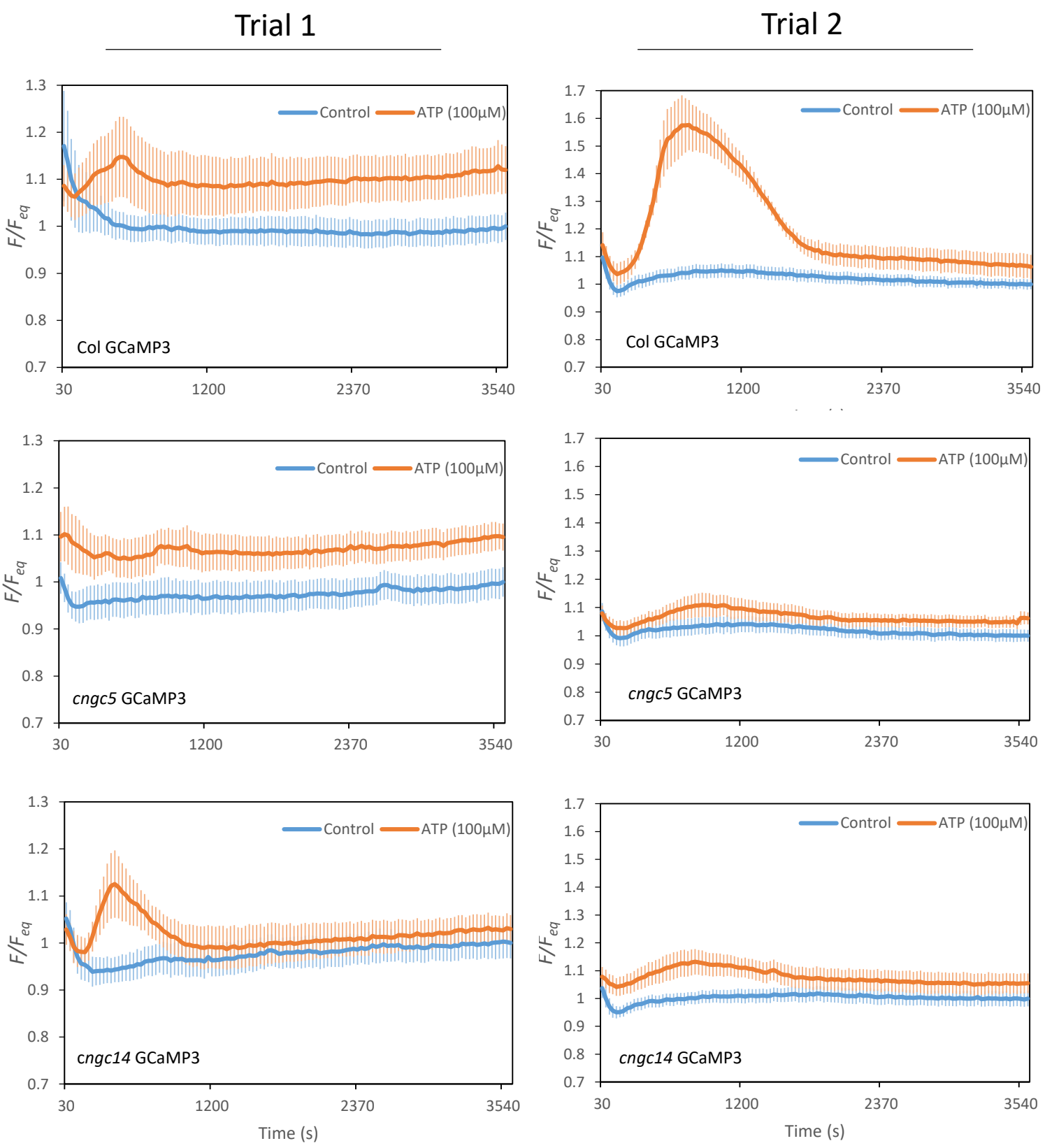

Figure A2.3: *CNGC5* and *CNGC14* may be involved in DAMP-induced Ca^{2+} response. Homozygous *cngc5* GCaMP3 and *cngc14* GCaMP3 were induced with WI control (blue) or 100µM ATP. n=5. Error bars represent ±SE. Two trials were conducted.

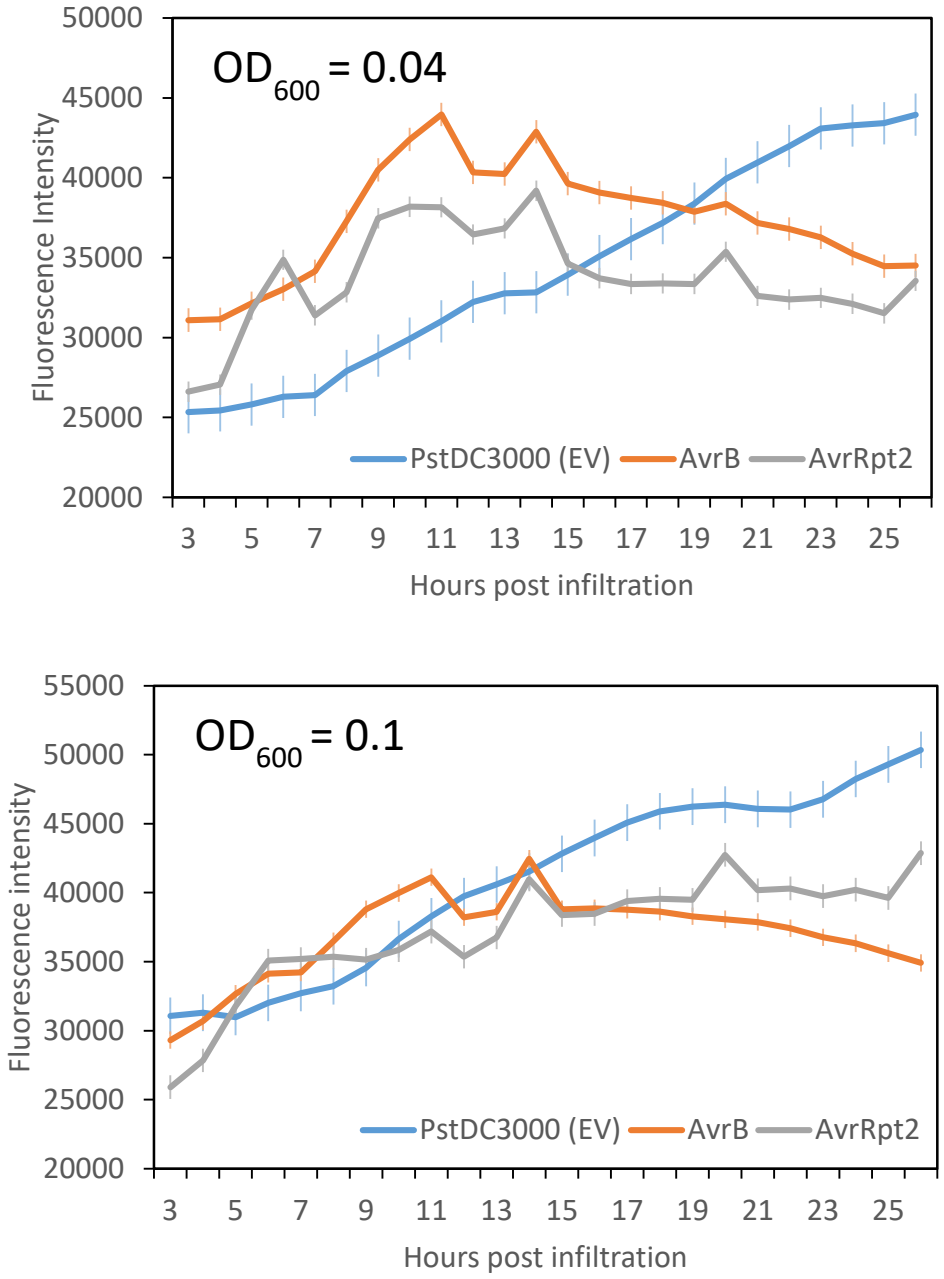

Figure A2.4: *Pseudomonas syringae* effectors AvrB and AvrRpt2 induce Ca^{2+} response best at OD_{600} of 0.04. Transgenic GCaMP3 *A, thaliana* leaves were infiltrated with PstDC3000 (Empty vector (EV)), AvrB, or AvrRpt2 at the respective growth optimal density (OD). Leaves were immediately cored and normalized in 100µl water for 3 hours before measuring in the plate reader n=5. Error bars represent ±SE. Only one trial was conducted.

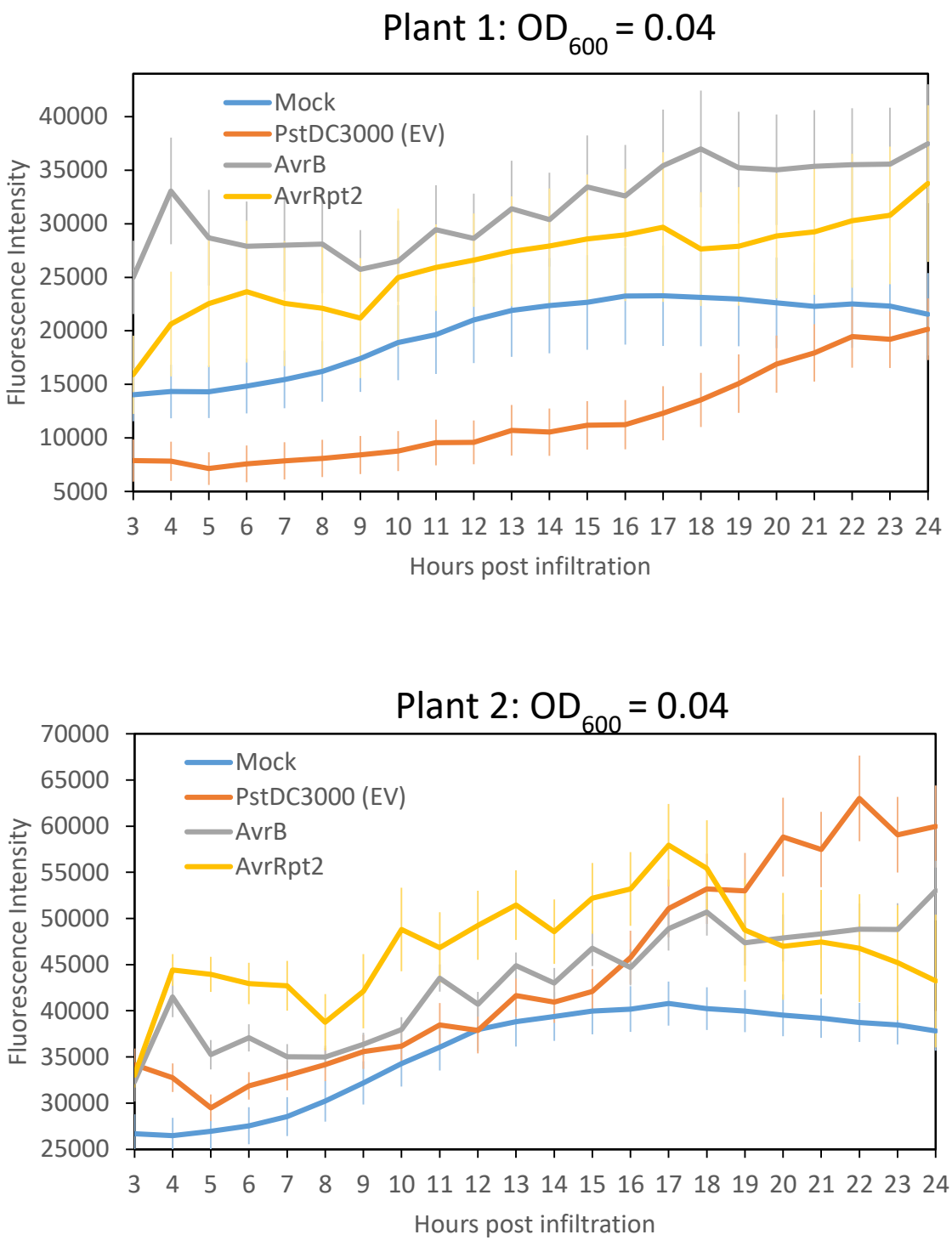

Figure A2.5: *Pseudomonas syringae* effectors AvrB and AvrRpt2 induce Ca^{2+} response. Transgenic GCaMP3 *A, thaliana* leaves were infiltrated with PstDC3000 (Empty vector (EV)), AvrB, or AvrRpt2, or mock ($MgCl_2$) at the respective growth optimal density (OD). Leaves were immediately cored and normalized in 100µl water for 3 hours before measuring in the plate-reader n=5. Error bars represent ±SE. Two experimental trials were conducted.

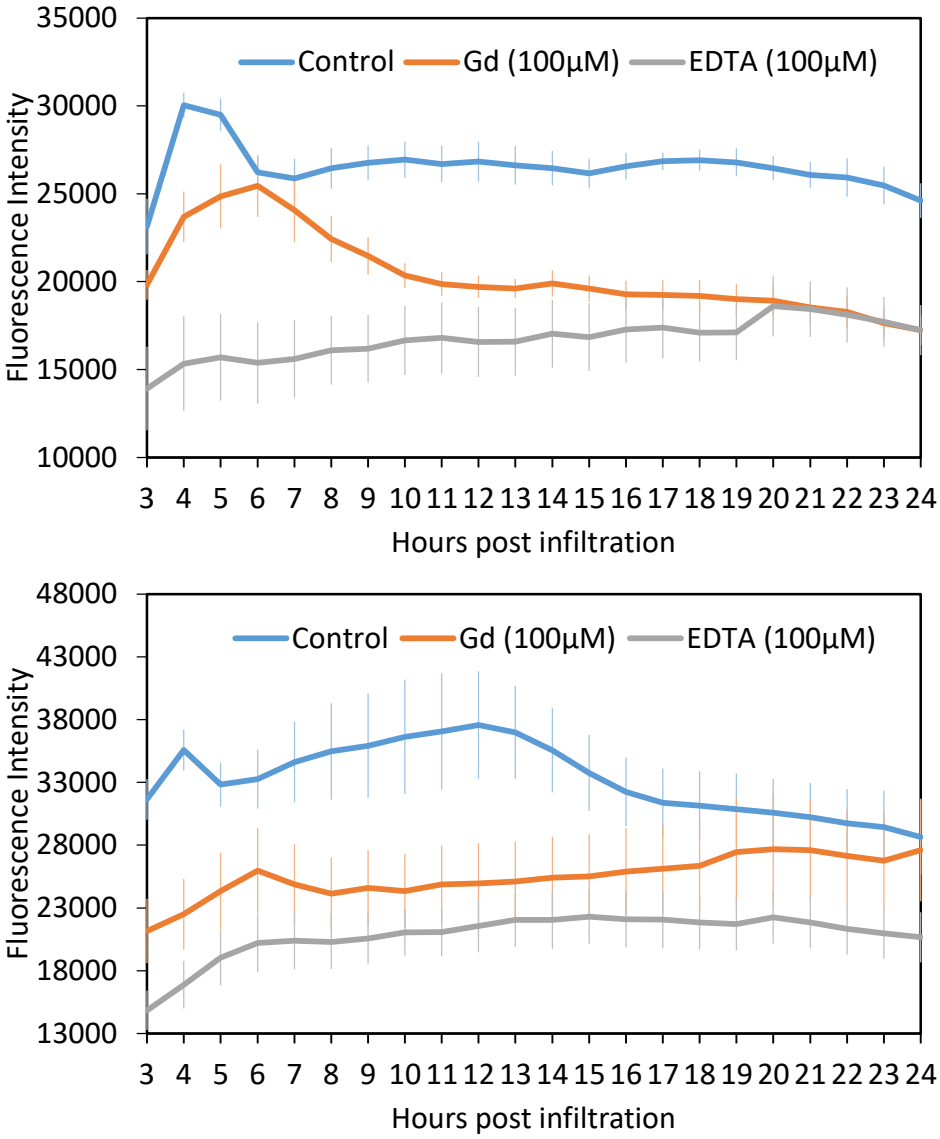

Figure A2.6: Ca^{2+} chelator, EDTA and Ca^{2+} channel blocker, gadolinium (Gd) reduces Ca^{2+} signal induced by *Pseudomonas syringae* effector AvrB. Transgenic GCaMP3 *A. thaliana* leaves were infiltrated with AvrB at the OD_{600} of 0.04. Leaves were immediately cored and normalized in equal amount of water, 100µM Gd or 100µM EDTA for 3 hours before measuring in the plate reader for 24 hours. n=5. Error bars represent ±SE. Two experimental trials were conducted.

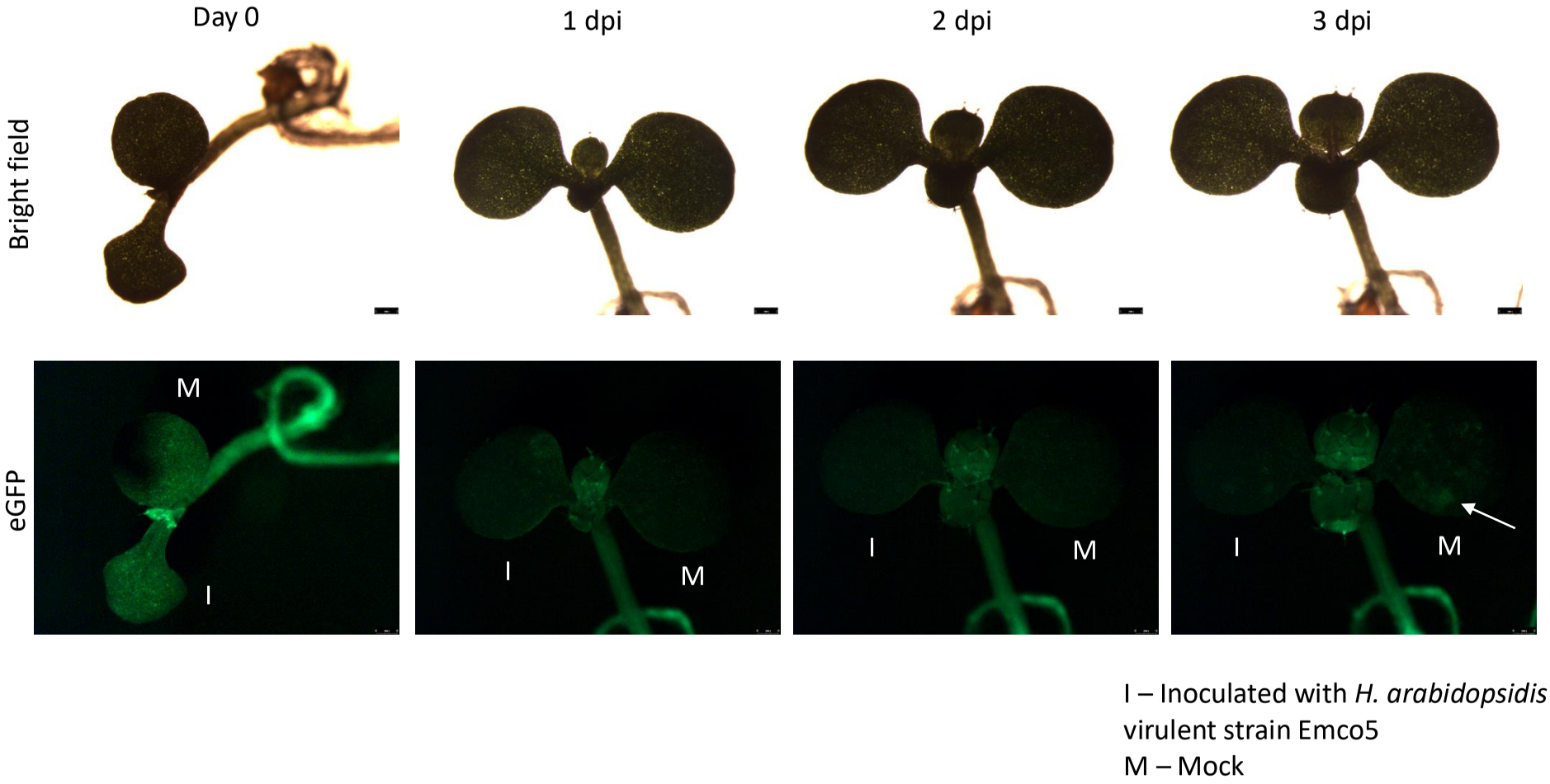

Figure A2.7: An elevation of Ca^{2+} signals in cotyledons induced by virulent *H. arabidopsidis* strain Emco5, 3 dpi. 11 day old GCaMP3 transgenic seedlings were inoculated with virulent strain of *H. arabidopsidis* Emco5 (I) or mock water (M). n=2. Scale bar = 1 mm. Image contrast increased by 70%.